Commun Nonlinear Sci Numer Simulat 145 (2025) 108724

Contents lists available at ScienceDirect

Communications in Nonlinear Science and Numerical Simulation

journal homepage: www.elsevier.com/locate/cnsns

Research paper

Stability and error analysis of linear IMEX schemes for sixth-order Cahn–Hilliard-type equations

Nan Zheng [a,c,1], Jie Shen [b,c,*,1]

[a] Department of Applied Mathematics, The Hong Kong Polytechnic University, Hung Hom, Kowloon, Hong Kong
[b] School of Mathematical Science, Eastern Institute of Technology, Ningbo, China
[c] School of Mathematical Sciences and Fujian Provincial Key Laboratory on Mathematical Modeling and High Performance Scientific Computing, Xiamen University, Xiamen, Fujian, 361005, China

ARTICLE INFO

MSC:
65M12
65M70
35J05
35K35

Keywords:
Sixth-order Cahn–Hilliard-type equations
IMEX schemes
High-order
Unconditional stability
Error analysis

ABSTRACT

In this paper, we develop efficient implicit-explicit (IMEX) schemes for solving sixth-order Cahn–Hilliard-type equations based on the generalized scalar auxiliary variable (GSAV) approach. These novel schemes provide several remarkable advantages: (i) they are linear and only require solving one elliptic equation with constant coefficients at each time step; (ii) they are unconditionally energy stable and yield a uniform bound for the numerical solution. We also establish rigorous error estimates of up to fifth-order for these schemes, and present various numerical experiments to validate the stability and accuracy of the proposed schemes.

1. Introduction

We consider the following energy functional [1,2]:

$$E(u) = \int_\Omega \left[\frac{1}{2} \left| -\epsilon^2 \Delta u + f(u) \right|^2 + \eta \left(\frac{\epsilon^2}{2} |\nabla u|^2 + F(u) \right) \right] d\boldsymbol{x}, \tag{1.1}$$

where the parameter $\epsilon > 0$ denotes the interfacial width, and $F(u)$ is a configuration potential function defined as $F(u) = \frac{1}{4}(u^2-1)^2$, with its derivative denoted by $f(u) = F'(u)$. It is important to note that the model parameter $\eta \in \mathbb{R}$ and the sign of η hold significance in both modeling and applications: For $\eta = 0$, the energy functional $E(u)$ corresponds to the well-known Willmore functional [3,4], which approximates the Canham–Helfrich bending surface energy, and has been effectively utilized in the study of deformations of elastic vesicles [5–7]; For $\eta > 0$, $E(u)$ is the Willmore regularization of the Cahn–Hilliard energy (CHW) [8,9] which has been used to investigate the significant anisotropy effects that arise during the growth and coarsening of thin films; For $\eta < 0$, $E(u)$ is the functionalized Cahn–Hilliard (FCH) free energy [10,11], which describes the characteristics of the amphiphilic polymer phase at the interface.

* Corresponding author at: School of Mathematical Science, Eastern Institute of Technology, Ningbo, China.
E-mail addresses: nanzheng@polyu.edu.hk (N. Zheng), jshen@eitech.edu.cn (J. Shen).
[1] The authors made equal contributions to this paper.

https://doi.org/10.1016/j.cnsns.2025.108724
Received 1 October 2024; Received in revised form 17 February 2025; Accepted 17 February 2025
Available online 28 February 2025

We study the following gradient flow equations associated with the free energy given by (1.1):

$$\begin{cases} \partial_t u = \mathcal{M}\Delta\mu, & t > 0,\ \boldsymbol{x} \in \Omega, \\ \mu = -\epsilon^2\Delta\omega + f'(u)\omega + \eta\omega, & t > 0,\ \boldsymbol{x} \in \Omega, \\ \omega = -\epsilon^2\Delta u + f(u), & t > 0,\ \boldsymbol{x} \in \Omega, \end{cases} \tag{1.2}$$

subject to either

the periodic boundary conditions, (1.3)

or the homogeneous Neumann boundary conditions:

$$\partial_{\mathbf{n}} u = \partial_{\mathbf{n}}\mu = \partial_{\mathbf{n}}\omega = 0, \text{ on } \partial\Omega, \tag{1.4}$$

and the initial condition is given by $u|_{t=0} = u_0(\boldsymbol{x}),\ \boldsymbol{x} \in \Omega$. The function μ denotes the chemical potential, defined as the first variational derivative of the energy functional in (1.1). Similarly, the first variational derivative of the Cahn–Hilliard free energy, as referenced in [12], is represented by ω. In the above system, $\mathcal{M} > 0$ represents a mobility constant. By taking the inner product of the first equation in (1.2) with μ, the second and the last equations in (1.2) with $\partial_t u$, we can derive the following energy dissipation law:

$$\frac{d}{dt}E(u) = -\mathcal{M}\|\nabla\mu\|^2. \tag{1.5}$$

The system (1.2) consists of three coupled second-order equations. It can alternatively be formulated as a sixth-order Cahn–Hilliard-type equation for the variable u. Numerical approximation of the system is very challenging due to the high-order derivatives and nonlinearity. Several attempts have been made in the literature to develop efficient and accurate numerical schemes for Eq. (1.2). For instance, in [13,14], the authors proposed semi-implicit schemes with a linear stabilizer, which are conditionally energy stable. Additionally, a fully implicit scheme based on the convex splitting approach was considered in [8,15], which includes a convergence analysis. More recently, the authors of [2,9,16] proposed linear, unconditional energy stability schemes based on the original scalar auxiliary variable approach [17,18]. However, their error analysis is not yet available, and it is not clear how to extend these schemes to higher-order while keeping the energy stability.

The primary objective of this paper is to develop a class of high-order IMEX schemes for (1.2) using the generalized SAV (GSAV) approach [19,20] and carry out the corresponding error analysis. Our contributions can be summarized as follows:

- We develop a class of high-order IMEX schemes which possess several notable advantages: (i) firstly, they are purely linear and only require solving a single elliptic equation with constant coefficients at each time step; (ii) secondly, they satisfy a modified energy dissipation law, and their numerical solutions are unconditionally bounded.
- We perform a rigorous error analysis for these schemes up to fifth-order in a unified framework.

Due to the highly nonlinear nature, the error analysis here is significantly more challenging than the one in [20]. To the best of our knowledge, these are the first error analyses for higher-order numerical schemes for the sixth-order Cahn–Hilliard-type Eq. (1.2). While this analysis is established for the semi-discrete (in time) schemes, it is expected that error estimates for fully discrete schemes with consistent Galerkin type spatial discretization can also be derived.

The remainder of the paper is organized as follows. In Section 2, we develop a class of IMEX-GSAV schemes, and derive an unconditional bound for their numerical solutions. In Section 3, we conduct a rigorous error analysis for the newly proposed schemes up to fifth-order in a unified framework. We then present some numerical experiments in Section 4, followed by some concluding remarks in Section 5.

2. New IMEX schemes based on the GSAV approach

In this section, we construct a class of new IMEX schemes based on the GSAV approach for the six-order Cahn–Hilliard-type Eq. (1.2), and show that their numerical solutions are uniformly bounded.

Introducing an SAV $r(t) = E(u) + L_0$ where $L_0 > 0$ so that $r(t) \geq 1 > 0$, we expand the system (1.2) with the energy dissipation law (1.5) as follows [19,21]:

$$\begin{cases} \partial_t u = \mathcal{M}\Delta\mu, & t > 0,\ \boldsymbol{x} \in \Omega, \\ \mu = -\epsilon^2\Delta\omega + f'(u)\omega + \eta\omega, & t > 0,\ \boldsymbol{x} \in \Omega, \\ \omega = -\epsilon^2\Delta u + f(u), & t > 0,\ \boldsymbol{x} \in \Omega, \\ d_t r = -\mathcal{M}\dfrac{r(t)}{E(u) + L_0}\|\nabla\mu\|^2, \end{cases} \tag{2.1}$$

where the boundary conditions for $u,\ \mu,\ \omega$ are either (1.3) or (1.4). Note that the solution of (1.2) is a solution of the above system with $r(0) = E(u|_{t=0}) + L_0$.

Following [21], we construct the kth-order ($1 \le k \le 6$) IMEX schemes for arbitrary $\eta \in \mathbb{R}$ in a uniform way as follows:

$$\begin{aligned}
&\frac{\alpha_k \bar{u}^{n+1} - A_k(u^n)}{\Delta t} = \mathcal{M}\Delta\bar{\mu}^{n+1},\\
&\bar{\mu}^{n+1} = -\epsilon^2\Delta\bar{\omega}^{n+1} + (f'(B_k(\bar{u}^n)) + \eta)B_k(\bar{\omega}^n),\\
&\bar{\omega}^{n+1} = -\epsilon^2\Delta\bar{u}^{n+1} + f(B_k(\bar{u}^n)),
\end{aligned} \tag{2.2a}$$

$$\frac{r^{n+1} - r^n}{\Delta t} = -\mathcal{M}\frac{r^{n+1}}{E(\bar{u}^{n+1}) + L_0}\|\nabla\bar{\mu}^{n+1}\|^2, \tag{2.2b}$$

$$\xi^{n+1} = \frac{r^{n+1}}{E(\bar{u}^{n+1}) + L_0}, \tag{2.2c}$$

$$u^{n+1} = \eta_k^{n+1}\bar{u}^{n+1} \text{ with } \eta_k^{n+1} = 1 - (1 - \xi^{n+1})^{k+1}. \tag{2.2d}$$

where the boundary conditions for u^{n+1}, μ^{n+1}, ω^{n+1} are either

the periodic boundary conditions, (2.3)

or the no-flux type as:

$$\partial_{\mathbf{n}}u^{n+1} = \partial_{\mathbf{n}}\mu^{n+1} = \partial_{\mathbf{n}}\omega^{n+1} = 0. \tag{2.4}$$

In the above, α_k, A_k and B_k are given by:
first-order:

$$\alpha_1 = 1, \quad A_1(u^n) = u^n, \quad B_1(\bar{u}^n) = \bar{u}^n;$$

second-order:

$$\alpha_2 = \frac{3}{2}, \quad A_2(u^n) = 2u^n - \frac{1}{2}u^{n-1}, \quad B_2(\bar{u}^n) = 2\bar{u}^n - \bar{u}^{n-1};$$

third-order:

$$\alpha_3 = \frac{11}{6}, \quad A_3(u^n) = 3u^n - \frac{3}{2}u^{n-1} + \frac{1}{3}u^{n-2}, \quad B_3(\bar{u}^n) = 3\bar{u}^n - 3\bar{u}^{n-1} + \bar{u}^{n-2}.$$

fourth-order:

$$\alpha_4 = \frac{25}{12}, \quad A_4(u^n) = 4u^n - 3u^{n-1} + \frac{4}{3}u^{n-2} - \frac{1}{4}u^{n-3}, \quad B_4(\bar{u}^n) = 4\bar{u}^n - 6\bar{u}^{n-1} + 4\bar{u}^{n-2} - \bar{u}^{n-3};$$

fifth-order:

$$\begin{aligned}
\alpha_5 = \frac{137}{60}, \quad A_5(u^n) &= 5u^n - 5u^{n-1} + \frac{10}{3}u^{n-2} - \frac{5}{4}u^{n-3} + \frac{1}{5}u^{n-4},\\
B_5(\bar{u}^n) &= 5\bar{u}^n - 10\bar{u}^{n-1} + 10\bar{u}^{n-2} - 5\bar{u}^{n-3} + \bar{u}^{n-4};
\end{aligned}$$

sixth-order:

$$\begin{aligned}
\alpha_6 = \frac{147}{60}, \quad A_6(u^n) &= 6u^n - \frac{15}{2}u^{n-1} + \frac{20}{3}u^{n-2} - \frac{15}{4}u^{n-3} + \frac{6}{5}u^{n-4} - \frac{1}{6}u^{n-5},\\
B_6(\bar{u}^n) &= 6\bar{u}^n - 15\bar{u}^{n-1} + 20\bar{u}^{n-2} - 15\bar{u}^{n-3} + 6\bar{u}^{n-4} - \bar{u}^{n-5}.
\end{aligned}$$

Note that (2.2b)–(2.2d) can be carried out directly without solving any differential equations. Therefore the main computational cost is in (2.2a) which is a system with three coupled second-order equations with constant coefficients in the following form:

$$\begin{aligned}
&\alpha\bar{u} - \mathcal{M}\Delta\bar{\mu} = \bar{f},\\
&\bar{\mu} + \epsilon^2\Delta\bar{\omega} = \bar{g},\\
&\bar{\omega} + \epsilon^2\Delta\bar{u} = \bar{h},
\end{aligned} \tag{2.5}$$

with either periodic boundary conditions or the homogeneous Neumann boundary conditions.

- If the boundary conditions are periodic, by using the Fourier-spectral method in space, the coupled linear equations in (2.2a) in the frequency space reduce to a diagonal system so it can be easily solved. More precisely, by using the fast Fourier transform, the total cost of solving (2.2a) is $O(N^d log N)$ where N is the number of points in each direction and d is the dimension of the domain.
- On the other hand, if the boundary conditions are homogeneous Neumann for u, μ, ω, the coupled system (2.2a) can also be efficiently solved by using a matrix diagonalization method presented in [13] with the spectral-Galerkin approximation in space. The total cost is essentially the same as solving three decoupled second-order equations with constant coefficients.

In summary, we can obtain $\bar{u}^{n+1}$, r^{n+1}, ξ^{n+1} and u^{n+1} from (2.2) as follows:

- Solve $(\bar{u}^{n+1}, \bar{\mu}^{n+1}, \bar{\omega}^{n+1})$ from (2.2a);
- Determine r^{n+1} from (2.2b);
- Compute ξ^{n+1}, η_k^{n+1} and update u^{n+1} from (2.2c)–(2.2d).

2.1. A stability result

We show below that the numerical solution of (2.2) is uniformly bounded. To this end, we need to first establish a lower bound for the nonlinear part of the free energy.

Lemma 2.1. *Let* $E(u) = \int_\Omega [\frac{1}{4}\epsilon^4|\Delta u|^2 + \frac{\alpha}{2}u^2]d\boldsymbol{x} + E_1(u)$, *where*

$$E_1(u) := \int_\Omega \left[\frac{1}{4}\epsilon^4|\Delta u|^2 + (\frac{\eta}{2}-1)\epsilon^2|\nabla u|^2 + \frac{1}{2}f^2(u) + 3\epsilon^2u^2|\nabla u|^2 + \eta\tilde{F}(u) + \frac{\alpha^2-2\alpha\eta}{4\eta}\right] d\boldsymbol{x},$$

with $\alpha > 0$ *and* $\tilde{F}(u) = \frac{1}{4}(u^2 - 1 + \frac{\alpha}{\eta})^2$. *There exists* $L_0 > 0$ *such that* $E_1(u) \geq -L_0 + 1$ *for all* $u \in H^2(\Omega)$.

Proof. Since $f(u) = u^3 - u$, we have

$$\begin{aligned} E(u) &= \int_\Omega \left[\frac{1}{2}|-\epsilon^2\Delta u + f(u)|^2 + \eta\left(\frac{\epsilon^2}{2}|\nabla u|^2 + F(u)\right)\right] d\boldsymbol{x} \\ &= \int_\Omega \left[\frac{1}{2}\epsilon^4|\Delta u|^2 + (\frac{\eta}{2}-1)\epsilon^2|\nabla u|^2 + \frac{1}{2}f^2(u) - \epsilon^2u^3\Delta u + \eta F(u)\right] d\boldsymbol{x} \\ &= \int_\Omega \left[\frac{1}{2}\epsilon^4|\Delta u|^2 + \frac{\alpha}{2}u^2 + (\frac{\eta}{2}-1)\epsilon^2|\nabla u|^2 + \frac{1}{2}f^2(u) + 3\epsilon^2u^2|\nabla u|^2 + \eta\tilde{F}(u) + \frac{\alpha^2-2\alpha\eta}{4\eta}\right] d\boldsymbol{x} \\ &:= \int_\Omega [\frac{1}{4}\epsilon^4|\Delta u|^2 + \frac{\alpha}{2}u^2]d\boldsymbol{x} + E_1(u). \end{aligned} \tag{2.6}$$

Hence, if $\frac{\eta}{2} - 1 \geq 0$, we have $E_1(u) \geq 0$. On the other hand, if $\frac{\eta}{2} - 1 < 0$, we derive from integration by parts that

$$-\int_\Omega (\frac{\eta}{2}-1)\epsilon^2|\nabla u|^2 d\boldsymbol{x} = (\frac{\eta}{2}-1)\epsilon^2(\Delta u, u) \leq \int_\Omega \frac{1}{4}\epsilon^4|\Delta u|^2 + (\frac{\eta}{2}-1)^2u^2 d\boldsymbol{x}.$$

Since $f^2(u) = (u^3 - u)^2$, one easily derive from the above that there exists $L_0 > 0$ such that $E_1(u) \geq -L_0 + 1$. □

Theorem 2.1. *Given* $r^n \geq 0$, *we have* $r^{n+1} \geq 0$, $\xi^{n+1} \geq 0$, *and the schemes* (2.2) *are unconditionally energy stable in the sense that*

$$r^{n+1} - r^n \leq -\Delta t\mathcal{M}\xi^{n+1}\|\nabla\bar{\mu}^{n+1}\|^2 \leq 0. \tag{2.7}$$

Furthermore, there exists $M_k > 0$ *such that*

$$\|u^{n+1}\|_{H^2}^2 \leq M_k. \tag{2.8}$$

Proof. Given $r^n > 0$ and since $E(\bar{u}^{n+1}) + L_0 > 0$, it follows from (2.2b) that

$$r^{n+1} = \frac{r^n}{1 + \Delta t\mathcal{M}\frac{\|\nabla\bar{\mu}^{n+1}\|^2}{E(\bar{u}^{n+1})+L_0}} \geq 0.$$

Then we derive from (2.2c) that $\xi^{n+1} \geq 0$ and obtain (2.7).

Denote $M_0 := r^0 = E[u(\cdot, 0)]$, then (2.7) implies $r^n \leq M_0$.

Since $E_1(u) + L_0 \geq 1$ for all u. It then follows from (2.2c) that

$$|\xi^{n+1}| = \frac{r^{n+1}}{E(\bar{u}^{n+1}) + L_0} \leq \frac{M_0}{\frac{1}{4}\epsilon^4\|\Delta\bar{u}^{n+1}\|^2 + \frac{\alpha}{2}\|\bar{u}^{n+1}\|^2 + 1}. \tag{2.9}$$

Let $\eta_k^{n+1} = 1 - (1 - \xi^{n+1})^{k+1}$, we have $\eta_k^{n+1} = \xi^{n+1}P_k(\xi^{n+1})$ with P_k being a polynomial of degree k. Then, we derive that there exists $\tilde{M}_k > 0$ such that

$$|\eta_k^{n+1}| = |\xi^{n+1}P_k(\xi^{n+1})| \leq \frac{\tilde{M}_k}{\epsilon^4\|\Delta\bar{u}^{n+1}\|^2 + 2\alpha\|\bar{u}^{n+1}\|^2 + 4},$$

which, together with $u^{n+1} = \eta_k^{n+1}\bar{u}^{n+1}$, implies

$$\|\Delta u^{n+1}\|^2 = (\eta_k^{n+1})^2\|\Delta\bar{u}^{n+1}\|^2 \leq \left(\frac{\tilde{M}_k}{\epsilon^4\|\Delta\bar{u}^{n+1}\|^2 + 2\alpha\|\bar{u}^{n+1}\|^2 + 4}\right)^2\|\Delta\bar{u}^{n+1}\|^2 \leq (\frac{\tilde{M}_k}{\epsilon^2})^2, \tag{2.10}$$

$$\|u^{n+1}\|^2 = (\eta_k^{n+1})^2\|\bar{u}^{n+1}\|^2 \leq \left(\frac{\tilde{M}_k}{\epsilon^4\|\Delta\bar{u}^{n+1}\|^2 + 2\alpha\|\bar{u}^{n+1}\|^2 + 4}\right)^2\|\bar{u}^{n+1}\|^2 \leq (\frac{\tilde{M}_k}{2\alpha})^2, \tag{2.11}$$

using integration by parts and Cauchy inequality yields

$$\|\nabla u\|^2 = -(u, \Delta u) \leq \frac{1}{2}\|u\|^2 + \frac{1}{2}\|\Delta u\|^2 \leq (\frac{1}{2\epsilon^4} + \frac{1}{8\alpha^2})(\tilde{M}_k)^2, \tag{2.12}$$

which implies the desired result (2.8). □

3. Error analysis

We carry out a rigorous error analysis for the schemes (2.2) in this section. We first recall some preliminary lemmas, which will be extensively utilized in the subsequent analyses.

3.1. Some useful lemmas

Lemma 3.1 (*Interpolation Inequality [22,23]*). *Let $0 \le s_1 \le s_2$, $\theta \in (0,1)$ and $s = \theta s_1 + (1-\theta)s_2$. Then,*

$$\|u\|_{H^s(\Omega)} \le C\|u\|^{\theta}_{H^{s_1}(\Omega)}\|u\|^{1-\theta}_{H^{s_2}(\Omega)}.$$

Lemma 3.2 (*Discrete Grönwall's Inequalities [24,25]*). *Let $k > 0$ and $T > 0$, suppose that y^n, h^n, g^n, f^n are four nonnegative sequences satisfying*

$$y^m + k\sum_{n=0}^{m} h^n \le B + k\sum_{n=0}^{m}(g^n y^n + f^n), \text{with } k\sum_{n=0}^{T/k} g^n \le M, \quad \forall\ 0 \le m \le T/k.$$

If $kg^n < 1$, $\forall\ 0 \le n \le T/k$, then it holds that for $\sigma = \max_{0\le n\le T/k}(1-kg^n)^{-1}$,

$$y^m + k\sum_{n=1}^{m} h^n \le \exp(\sigma M)(B + k\sum_{n=0}^{m} f^n), \quad \forall m \le T/k.$$

Next, we recall a useful lemma by Nevanlinna and Odeh (1981) which plays a key role in our analysis.

Lemma 3.3 (*[26,27]*). *For $1 \le k \le 5$, there exists $0 \le \tau_k < 1$, a positive definite symmetric matrix $G = (g_{i,j}) \in \mathbb{R}^{k,k}$ and real numbers $\delta_0, \dots, \delta_k$ such that*

$$\begin{aligned}(\alpha_k u^{n+1} - A_k(u^n), u^{n+1} - \tau_k u^n) = &\sum_{i,j=1}^{k} g_{i,j}(u^{n+1+i-k}, u^{n+1+j-k}) \\ &- \sum_{i,j=1}^{k} g_{i,j}(u^{n+i-k}, u^{n+j-k}) + \left\|\sum_{i=0}^{k}\delta_i u^{n+1+i-k}\right\|^2,\end{aligned} \tag{3.1}$$

where the smallest possible values of τ_k are

$$\tau_1 = \tau_2 = 0,\ \tau_3 = 0.0836,\ \tau_4 = 0.2878,\ \tau_5 = 0.8160.$$

Remark 3.1. Note that Akrivis et al. [27] have introduced a novel multiplier which allowed them to extend Lemma 3.3 to the sixth-order BDF method. It is anticipated that the results in Theorems 2.1 and 3.1 can also be extended to the sixth-order by using the result in [27].

3.2. Error estimates

For the sake of simplicity, we fix the mobility constant $\mathcal{M} = 1$. In order to simplify the analysis, we first rewrite the system (1.2) (resp. the scheme (2.2a)) into a single equation with six-order derivatives:

$$\begin{aligned}\frac{\alpha_k\bar{u}^{n+1} - A_k(u^n)}{\Delta t} =&\epsilon^4\Delta^3\bar{u}^{n+1} - \epsilon^2\Delta^2 f(B_k(\bar{u}^n)) \\ &+ \Delta(f'(B_k(\bar{u}^n))B_k(\bar{\omega}^n)) + \eta\Delta B_k(\bar{\omega}^n).\end{aligned} \tag{3.2}$$

We denote

$$\bar{e}^n = \bar{u}^n - u(t^n), \quad e^n = u^n - u(t^n), \quad e_r^n = r^n - r(t^n).$$

The main result of this section is stated in the following theorem.

Theorem 3.1. *Assume that $u \in C(0,T;H^5(\Omega)) \cap H^k(0,T;H^4(\Omega)) \cap H^{k+1}(0,T;H^1(\Omega))$. Let $\bar{u}^q$ and u^q ($q = 1,\dots,k-1$) be determined by a proper kth order initialization procedure. Let $\bar{u}^{n+1}$ and u^{n+1} be computed with the kth order scheme (2.2) with*

$$\eta_1^{n+1} = 1 - (1-\xi^{n+1})^3, \quad \eta_k^{n+1} = 1 - (1-\xi^{n+1})^{k+1}\ (2 \le k \le 5).$$

Then we have

$$\|\bar{e}^{n+1}\|_{H^2}^2 + \|e^{n+1}\|_{H^2}^2 \le C\Delta t^{2k}, \quad 1 \le k \le 5,$$

where the constant C is independent of Δt.

Proof. As in [20], an essential step of the proof is to show that there exists an absolute constant C_0 independent of Δt such that

$$|1 - \xi^q| \le C_0\Delta t, \quad \forall q \le T/\Delta t, \tag{3.3}$$

by using an induction method with the help of a bootstrap argument.

When $q = 0$, (3.3) certainly holds. Assuming that $|1 - \xi^q| \le C_0\Delta t$ is valid for $\forall q \le m$, we shall prove by induction that

$$|1 - \xi^{m+1}| \le C_0\Delta t.$$

We shall first consider $k = 2, 3, 4, 5$ and indicate the necessary modifications for $k = 1$. The induction process consists of the following two steps.

Step 1: Bounds for $\|\bar{u}^{n+1}\|_{H^2}$ and $\|\bar{u}^{n+1}\|_{H^5}$ for all $0 \le n \le m$.

By following a similar procedure as outlined in [20], based on the induction assumption and using the given condition

$$\Delta t \le \min\{\frac{1}{2C_0^{k+1}}, 1\}, \tag{3.4}$$

we can readily obtain

$$|1 - \eta_k^q| \le \frac{\Delta t^k}{2}, \quad \forall q \le m.$$

By the assumptions on the exact solution u and (2.8), we can choose C large enough such that for any $t \le T$ and $q \le m$, we have

$$\|u(t)\|_{H^5} \le C, \quad \|\bar{u}^q\|_{H^2} \le C. \tag{3.5}$$

Due to $H^2 \subseteq L^\infty$, we can assume that C also satisfies

$$|f^{(i)}(u(t))|_{L^\infty} \le C, \quad |f^{(i)}(\bar{u}^q)|_{L^\infty} \le C, \quad i = 0, 1, 2, 3. \tag{3.6}$$

By subtracting Eq. (2.2a) from Eq. (1.2) at t^{n+1}, we obtain an error equation that corresponds to

$$\alpha_k\bar{e}^{n+1} - A_k(\bar{e}^n) = A_k(u^n) - A_k(\bar{u}^n) + \epsilon^4\Delta t\Delta^3\bar{e}^{n+1} + R_k^n + \epsilon^2\Delta t\sum_{i=1}^{3}\Delta Q_i^n, \tag{3.7}$$

where

$$\begin{aligned}
Q_1^n &= -\Delta f(B_k(\bar{u}^n)) + \Delta f(u(t^{n+1})),\\
Q_2^n &= \frac{1}{\epsilon^2}f'(B_k(\bar{u}^n))B_k(\bar{\omega}^n) - \frac{1}{\epsilon^2}f'(u(t^{n+1}))\omega(t^{n+1}),\\
Q_3^n &= \frac{\eta}{\epsilon^2}B_k(\bar{\omega}^n) - \frac{\eta}{\epsilon^2}\omega(t^{n+1}),
\end{aligned}$$

and truncation error defined by

$$\begin{aligned}
R_k^n &= \Delta t\left(\partial_t u(t^{n+1}) - \frac{\alpha_k u(t^{n+1}) - A_k(u(t^n))}{\Delta t}\right)\\
&= \sum_{i=1}^{k}\delta_i\int_{t^{n+1-i}}^{t^{n+1}}(t^{n+1-i} - s)^k\frac{\partial^{k+1}u}{\partial t^{k+1}}(s)ds,
\end{aligned} \tag{3.8}$$

where δ_i are some fixed positive constants.

Using Lemma 3.3 and taking the inner product of (3.7) with $\Delta^2\bar{e}^{n+1} - \tau_k\Delta^2\bar{e}^n$ lead to

$$\begin{aligned}
&\sum_{i,j=1}^{k} g_{ij}(\Delta\bar{e}^{n+1+i-k}, \Delta\bar{e}^{n+1+j-k}) - \sum_{i,j=1}^{k} g_{ij}(\Delta\bar{e}^{n+i-k}, \Delta\bar{e}^{n+j-k})\\
&+ \|\sum_{i=0}^{k}\delta_i\Delta\bar{e}^{n+1+i-k}\|^2 + \epsilon^4\Delta t\|\nabla\Delta^2\bar{e}^{n+1}\|^2\\
=&(\Delta A_k(u^n) - \Delta A_k(\bar{u}^n), \Delta\bar{e}^{n+1} - \tau_k\Delta\bar{e}^n) - \epsilon^4\Delta t(\Delta^3\bar{e}^{n+1}, \tau_k\Delta^2\bar{e}^n)\\
&+ (\nabla R_k^n, -\nabla\Delta\bar{e}^{n+1} + \tau_k\nabla\Delta\bar{e}^n) + \epsilon^2\Delta t\sum_{i=1}^{3}(\Delta Q_i^n, \Delta^2\bar{e}^{n+1} - \tau_k\Delta^2\bar{e}^n)\\
=&I_1 + I_2 + I_3 + I_4 + I_5 + I_6,
\end{aligned} \tag{3.9}$$

where I_4, I_5, I_6 denote respectively the three terms in the summation. Next, we need to derive proper bounds for the terms I_j $(j = 1, \dots, 6)$ such that we can eventually apply the discrete Grönwall Lemma to derive the desired stability. This process is

very tedious. For the sake of readability, we move the details to Appendix.

Combining (3.9) (A.1), (A.3), (A.5) and (A.8) derived in the Appendix in (3.9), we have

$$\begin{aligned}
&\sum_{i,j=1}^{k} g_{ij}(\Delta\bar{e}^{n+1+i-k}, \Delta\bar{e}^{n+1+j-k}) - \sum_{i,j=1}^{k} g_{ij}(\Delta\bar{e}^{n+i-k}, \Delta\bar{e}^{n+j-k}) \\
&+ \|\sum_{i=0}^{k} \delta_i \Delta\bar{e}^{n+1+i-k}\|^2 + \frac{\epsilon^4\Delta t}{2}(\|\nabla\Delta^2\bar{e}^{n+1}\|^2 - \tau_k^2\|\nabla\Delta^2\bar{e}^{n}\|^2) \\
\le& CC_0^{2k+1}\Delta t^{2k+1} + C\Delta t^{2k}\int_{t^{n+1-k}}^{t^{n+1}} \|\nabla\frac{\partial^{k+1}u}{\partial t^{k+1}}(s)\|^2 ds + C\Delta t^{2k}\int_{t^{n+1-k}}^{t^{n+1}} \|\frac{\partial^{k}u}{\partial t^{k}}(s)\|_{H^4}^2 ds \\
&+ C\Delta t\left(\|B_k(\bar{e}^n)\|^2 + \|\nabla B_k(\bar{e}^n)\|^2 + \|\Delta B_k(\bar{e}^n)\|^2 + \|\nabla\Delta B_k(\bar{e}^n)\|^2 + \|\Delta^2 B_k(\bar{e}^n)\|^2\right) \\
&+ 3\epsilon^2\Delta t\|\Delta^2\bar{e}^{n+1}\|^2 + \frac{\epsilon^2\Delta t}{2}(\|\nabla\Delta\bar{e}^{n+1}\|^2 + \|\nabla\Delta\bar{e}^{n}\|^2).
\end{aligned} \tag{3.10}$$

Using the interpolation inequality in Lemma 3.1, we have

$$\begin{aligned}
&\sum_{i,j=1}^{k} g_{ij}(\Delta\bar{e}^{n+1+i-k}, \Delta\bar{e}^{n+1+j-k}) - \sum_{i,j=1}^{k} g_{ij}(\Delta\bar{e}^{n+i-k}, \Delta\bar{e}^{n+j-k}) \\
&+ \|\sum_{i=0}^{k} \delta_i \Delta\bar{e}^{n+1+i-k}\|^2 + \frac{\epsilon^4\Delta t}{2}(\|\nabla\Delta^2\bar{e}^{n+1}\|^2 - \tau_k^2\|\nabla\Delta^2\bar{e}^{n}\|^2) \\
\le& CC_0^{2k+1}\Delta t^{2k+1} + C\Delta t^{2k}\int_{t^{n+1-k}}^{t^{n+1}} \|\nabla\frac{\partial^{k+1}u}{\partial t^{k+1}}(s)\|^2 ds + C\Delta t^{2k}\int_{t^{n+1-2k}}^{t^{n+1}} \|\frac{\partial^{k}u}{\partial t^{k}}(s)\|_{H^4}^2 ds \\
&+ C\Delta t\left(\|B_k(\bar{e}^n)\|^2 + \|\nabla B_k(\bar{e}^n)\|^2 + \|\Delta B_k(\bar{e}^n)\|^2\right) + \frac{\epsilon^4\Delta t}{2}\frac{1-\tau_k^2}{2k+1}\sum_{i=0}^{k}\|\nabla\Delta^2\bar{e}^{n+1-i}\|^2.
\end{aligned} \tag{3.11}$$

Taking the sum on $\|\nabla\Delta^2\bar{e}^{n+1}\|^2 - \tau_k^2\|\nabla\Delta^2\bar{e}^{n}\|^2$ over the index n, we derive

$$\begin{aligned}
&\sum_{q=k-1}^{m}\left(\|\nabla\Delta^2\bar{e}^{q+1}\|^2 - \tau_k^2\|\nabla\Delta^2\bar{e}^{q}\|^2\right) \\
=&\frac{k(1-\tau_k^2)}{2k+1}\sum_{q=k-1}^{m}\|\nabla\Delta^2\bar{e}^{q+1}\|^2 + \sum_{q=k-1}^{m}(\frac{k\tau_k^2+k+1}{2k+1}\|\nabla\Delta^2\bar{e}^{q+1}\|^2 - \tau_k^2\|\nabla\Delta^2\bar{e}^{q}\|^2) \\
\ge&\frac{k(1-\tau_k^2)}{2k+1}\sum_{q=k-1}^{m}\|\nabla\Delta^2\bar{e}^{q+1}\|^2 + \sum_{q=k-1}^{m}\frac{1-\tau_k^2}{2k+1}\sum_{i=0}^{k}\|\nabla\Delta^2\bar{e}^{q+1-i}\|^2.
\end{aligned}$$

Then, we can take the sum of (3.11) over n from $k-1$ to m to obtain

$$\begin{aligned}
&\lambda_G\|\Delta\bar{e}^{m+1}\|^2 + \frac{\epsilon^4\Delta t}{2}\frac{k(1-\tau_k^2)}{2k+1}\sum_{q=0}^{m}\|\nabla\Delta^2\bar{e}^{q+1}\|^2 \\
&\le \sum_{i,j=1}^{k} g_{ij}(\Delta\bar{e}^{m+1+i-k}, \Delta\bar{e}^{m+1+j-k}) + \frac{\epsilon^4\Delta t}{2}\frac{k(1-\tau_k^2)}{2k+1}\sum_{q=0}^{m}\|\nabla\Delta^2\bar{e}^{q+1}\|^2 \\
&\le C\Delta t\sum_{q=0}^{m+1}\|\bar{e}^q\|_{H^2}^2 + C\Delta t^{2k}\int_0^T(\|\nabla\frac{\partial^{k+1}u}{\partial t^{k+1}}(s)\|^2 + \|\frac{\partial^{k}u}{\partial t^{k}}(s)\|_{H^4}^2 + C_0^{2k+2})ds,
\end{aligned} \tag{3.12}$$

where λ_G is the minimum eigenvalue of $G = (g_{ij})$.

By using a similar process, we can obtain bounds on $\|\nabla\bar{e}^{m+1}\|$ and $\|\bar{e}^{m+1}\|$.

Then, taking the inner product of (3.7) with $-\Delta\bar{e}^{n+1} + \tau_k\Delta\bar{e}^{n}$, we find that

$$\begin{aligned}
&\sum_{i,j=1}^{k} g_{ij}(\nabla\bar{e}^{n+1+i-k}, \nabla\bar{e}^{n+1+j-k}) - \sum_{i,j=1}^{k} g_{ij}(\nabla\bar{e}^{n+i-k}, \nabla\bar{e}^{n+j-k}) \\
&+ \|\sum_{i=0}^{k}\delta_i\nabla\bar{e}^{n+1+i-k}\|^2 + \epsilon^4\Delta t\|\Delta^2\bar{e}^{n+1}\|^2 \\
=&(A_k(u^n) - A_k(\bar{u}^n), -\Delta\bar{e}^{n+1} + \tau_k\Delta\bar{e}^{n}) + \epsilon^4\Delta t(\Delta^3\bar{e}^{n+1}, \tau_k\Delta\bar{e}^{n}) \\
&+ (R_k^n, -\Delta\bar{e}^{n+1} + \tau_k\Delta\bar{e}^{n}) + \epsilon^2\Delta t\left(\Delta(Q_1^n + Q_2^n + Q_3^n), -\Delta\bar{e}^{n+1} + \tau_k\Delta\bar{e}^{n}\right) \\
\le& CC_0^{2k+1}\Delta t^{2k+1} + \Delta t\|\nabla\bar{e}^{n+1}\|^2 + \Delta t\|\nabla\bar{e}^{n}\|^2 + \frac{\epsilon^4\Delta t}{2}(\|\Delta^2\bar{e}^{n+1}\|^2 + \tau_k^2\|\Delta^2\bar{e}^{n}\|^2) \\
&+ C\Delta t^{2k}\int_{t^{n+1-k}}^{t^{n+1}}\|\nabla\frac{\partial^{k+1}u}{\partial t^{k+1}}(s)\|^2 ds + \Delta t\|\nabla\bar{e}^{n+1}\|^2 + \Delta t\|\nabla\bar{e}^{n}\|^2
\end{aligned} \tag{3.13}$$

$$+\frac{\epsilon^2}{2}\Delta t\left(\|\nabla Q_1^k+\nabla Q_2^k+\nabla Q_3^k\|^2+2\|\nabla\Delta\bar{e}^{n+1}\|^2+2\|\nabla\Delta\bar{e}^{n}\|^2\right).$$

We can estimate the last term on the right-hand side of (3.13) as follows

$$\begin{aligned}
&\frac{\epsilon^2}{2}\Delta t\left(\|\nabla Q_1^k+\nabla Q_2^k+\nabla Q_3^k\|^2+2\|\nabla\Delta\bar{e}^{n+1}\|^2+2\|\nabla\Delta\bar{e}^{n}\|^2\right) \\
\le&\frac{3\epsilon^2}{2}\Delta t(\|\nabla Q_1^k\|^2+\|\nabla Q_2^k\|^2+\|\nabla Q_3^k\|^2)+\epsilon^2\Delta t\|\nabla\Delta\bar{e}^{n+1}\|^2+\epsilon^2\Delta t\|\nabla\Delta\bar{e}^{n}\|^2 \\
\le&C\Delta t\left(\|B_k(\bar{e}^n)\|^2+\|\nabla B_k(\bar{e}^n)\|^2+\|\Delta B_k(\bar{e}^n)\|^2+\|\nabla\Delta B_k(\bar{e}^n)\|^2\right) \\
&+C\Delta t^{2k}\int_{t^{n+1-2k}}^{t^{n+1}}\|\frac{\partial^k u}{\partial t^k}(s)\|_{H^3}^2 ds+\epsilon^2\Delta t\|\nabla\Delta\bar{e}^{n+1}\|^2+\epsilon^2\Delta t\|\nabla\Delta\bar{e}^{n}\|^2.
\end{aligned}\tag{3.14}$$

Combining (3.13) and (3.14), we have

$$\begin{aligned}
&\sum_{i,j=1}^{k} g_{ij}(\nabla\bar{e}^{n+1+i-k},\nabla\bar{e}^{n+1+j-k})-\sum_{i,j=1}^{k} g_{ij}(\nabla\bar{e}^{n+i-k},\nabla\bar{e}^{n+j-k}) \\
&+\|\sum_{i=0}^{k}\delta_i\nabla\bar{e}^{n+1+i-k}\|^2+\frac{\epsilon^4\Delta t}{2}\|\Delta^2\bar{e}^{n+1}\|^2 \\
\le&CC_0^{2k+1}\Delta t^{2k+1}+\Delta t\|\nabla\bar{e}^{n+1}\|^2+\Delta t\|\nabla\bar{e}^{n}\|^2+\frac{\epsilon^4\Delta t}{2}\tau_k^2\|\Delta^2\bar{e}^{n}\|^2 \\
&+C\Delta t\sum_{i=0}^{k-1}\left(\|\bar{e}^{n-i}\|^2+\|\nabla\bar{e}^{n-i}\|^2\right)+C\Delta t\sum_{i=0}^{k}\left(\|\Delta\bar{e}^{n+1-i}\|^2+\|\nabla\Delta\bar{e}^{n+1-i}\|^2\right) \\
&+C\Delta t^{2k}\int_{t^{n+1-k}}^{t^{n+1}}\|\nabla\frac{\partial^{k+1}u}{\partial t^{k+1}}(s)\|^2 ds+C\Delta t^{2k}\int_{t^{n+1-2k}}^{t^{n+1}}\|\frac{\partial^k u}{\partial t^k}(s)\|_{H^3}^2 ds.
\end{aligned}\tag{3.15}$$

Then, an application of the interpolation inequality leads to

$$\|\nabla\Delta\bar{e}^{n+1}\|\le\bar{C}\|\bar{e}^{n+1}\|_{H^1}^{1/3}\|\Delta^2\bar{e}^{n+1}\|^{2/3},$$

an application of Young's inequality leads to

$$\begin{aligned}
\|\nabla\Delta\bar{e}^{n+1}\|^2\le&\frac{512^2\bar{C}^6}{27\epsilon^8}\|\bar{e}^{n+1}\|_{H^1}^2+\frac{\epsilon^4}{256}\|\Delta^2\bar{e}^{n+1}\|^2 \\
\le&C\|\bar{e}^{n+1}\|_{H^1}^2+\frac{\epsilon^4}{256}\|\Delta^2\bar{e}^{n+1}\|^2.
\end{aligned}$$

Combining the above inequalities in (3.15), we obtain

$$\begin{aligned}
&\sum_{i,j=1}^{k} g_{ij}(\nabla\bar{e}^{n+1+i-k},\nabla\bar{e}^{n+1+j-k})-\sum_{i,j=1}^{k} g_{ij}(\nabla\bar{e}^{n+i-k},\nabla\bar{e}^{n+j-k}) \\
&+\|\sum_{i=0}^{k}\delta_i\nabla\bar{e}^{n+1+i-k}\|^2+\frac{\epsilon^4\Delta t}{2}(\|\Delta^2\bar{e}^{n+1}\|^2-\tau_k^2\|\Delta^2\bar{e}^{n}\|^2) \\
\le&CC_0^{2k+1}\Delta t^{2k+1}+C\Delta t\sum_{i=0}^{2k}\left(\|\bar{e}^{n+1-i}\|^2+\|\nabla\bar{e}^{n+1-i}\|^2\right)+\epsilon^4\Delta t\frac{1-\tau_k^2}{2(2k+1)}\sum_{i=0}^{2k}\|\Delta^2\bar{e}^{n+1-i}\|^2 \\
&+C\Delta t^{2k}\int_{t^{n+1-k}}^{t^{n+1}}\|\nabla\frac{\partial^{k+1}u}{\partial t^{k+1}}(s)\|^2 ds+C\Delta t^{2k}\int_{t^{n+1-2k}}^{t^{n+1}}\|\frac{\partial^k u}{\partial t^k}(s)\|_{H^3}^2 ds.
\end{aligned}$$

Taking the sum of the above over n from $k-1$ to m, we obtain

$$\begin{aligned}
\lambda_G\|\nabla\bar{e}^{m+1}\|^2\le&\sum_{i,j=1}^{k} g_{ij}(\nabla\bar{e}^{m+1+i-k},\nabla\bar{e}^{m+1+j-k}) \\
\le&C\Delta t\sum_{q=0}^{m+1}\|\bar{e}^{q}\|_{H^1}^2+C\Delta t^{2k}\int_0^T(\|\nabla\frac{\partial^{k+1}u}{\partial t^{k+1}}(s)\|^2+\|\frac{\partial^k u}{\partial t^k}(s)\|_{H^3}^2+C_0^{2k+2})ds.
\end{aligned}\tag{3.16}$$

Taking the inner product of (3.7) with $\bar{e}^{n+1}-\tau_k\bar{e}^{n}$, we arrive at

$$\sum_{i,j=1}^{k} g_{ij}(\bar{e}^{n+1+i-k}, \bar{e}^{n+1+j-k}) - \sum_{i,j=1}^{k} g_{ij}(\bar{e}^{n+i-k}, \bar{e}^{n+j-k})$$
$$+ \| \sum_{i=0}^{k} \delta_i \bar{e}^{n+1+i-k} \|^2 + \frac{\epsilon^4 \Delta t}{2}(\|\nabla \Delta \bar{e}^{n+1}\|^2 - \tau_k^2 \|\nabla \Delta \bar{e}^{n}\|^2)$$
$$\leq C C_0^{2k+1} \Delta t^{2k+1} + C\Delta t \sum_{i=0}^{2k} \|\bar{e}^{n+1-i}\|^2 + \epsilon^4 \Delta t \frac{1-\tau_k^2}{2(2k+1)} \sum_{i=0}^{2k} \|\nabla \Delta \bar{e}^{n+1-i}\|^2$$
$$+ C\Delta t^{2k} \int_{t^{n+1-k}}^{t^{n+1}} \| \frac{\partial^{k+1} u}{\partial t^{k+1}}(s)\|^2 ds + C\Delta t^{2k} \int_{t^{n+1-2k}}^{t^{n+1}} \| \frac{\partial^{k} u}{\partial t^{k}}(s)\|_{H^2}^2 ds.$$

Then taking the sum of above over n from $k-1$ to m, we have

$$\begin{aligned} \lambda_G \|\bar{e}^{m+1}\|^2 &\leq \sum_{i,j=1}^{k} g_{ij}(\bar{e}^{m+1+i-k}, \bar{e}^{m+1+j-k}) \\ &\leq C\Delta t \sum_{q=0}^{m+1} \|\bar{e}^{q}\|^2 + C\Delta t^{2k} \int_0^T \left(\| \frac{\partial^{k+1} u}{\partial t^{k+1}}(s)\|^2 + \| \frac{\partial^{k} u}{\partial t^{k}}(s)\|_{H^2}^2 + C_0^{2k+2} \right) ds. \end{aligned} \tag{3.17}$$

Summing up (3.12), (3.16) and (3.17), then using the discrete Grönwall's inequality in Lemma 3.2, we have

$$\|\bar{e}^{m+1}\|_{H^2}^2 + \epsilon^4 \Delta t \frac{k(1-\tau_k^2)}{4k+1} \sum_{q=0}^{m} \|\nabla \Delta^2 \bar{e}^{q+1}\|^2$$
$$\leq C exp((1-C\Delta t)^{-1}) \Delta t^{2k} \int_0^T (\| \frac{\partial^{k+1} u}{\partial t^{k+1}}(s)\|_{H^1}^2 + \| \frac{\partial^{k} u}{\partial t^{k}}(s)\|_{H^4}^2 + C_0^{2k+2}) ds$$
$$\leq C_2(1 + C_0^{2k+2}) \Delta t^{2k}.$$

Given that $0 < \epsilon^4 \frac{k(1-\tau_k^2)}{4k+1} < 1$, it follows that

$$\|\bar{e}^{n+1}\|_{H^2}, \quad (\Delta t \sum_{q=0}^{n} \|\nabla \Delta^2 \bar{e}^{q+1}\|^2)^{1/2} \leq \sqrt{C_2(1 + C_0^{2k+2})} \Delta t^k, \quad \forall\ 0 \leq n \leq m. \tag{3.18}$$

Then, combining (3.5) and (3.18), we obtain the following desired bounds:

$$\|\bar{u}^{n+1}\|_{H^2}, \ (\Delta t \sum_{q=0}^{n} \|\nabla \Delta^2 \bar{u}^{q+1}\|^2)^{1/2} \leq \bar{C}, \quad \forall\ 0 \leq n \leq m. \tag{3.19}$$

In addition, using the Sobolev embedding theorem, we can derive

$$|f^{(i)}(\bar{u}^{n+1})|_{L^\infty} \leq \bar{C}, \quad i = 0, 1, 2, 3, \quad \forall\ 0 \leq n \leq m. \tag{3.20}$$

Step 2: Estimate for $|1 - \xi^{m+1}|$. Thanks to (2.2b), we can get

$$e_r^{n+1} - e_r^n = \Delta t (\|\nabla \mu(u(t^{n+1}))\|^2 - \frac{r^{n+1}}{E(\bar{u}^{n+1})} \|\nabla \mu(\bar{u}^{n+1})\|^2) + R_1^n, \tag{3.21}$$

where

$$\mu = \epsilon^4 \Delta^2 u - \epsilon^2 f'(u) \Delta u - \eta \epsilon^2 \Delta u - \epsilon^2 \Delta f(u) + f'(u) f(u) + \eta f(u),$$

and

$$R_1^n = r(t^n) - r(t^{n+1}) + \Delta t r_t(t^{n+1}) = \int_{t^n}^{t^{n+1}} (s - t^n) r_{tt}(s) ds.$$

Direct calculation yields

$$r_{tt} = \int_\Omega (-\epsilon^2 \Delta u_t + f'(u) u_t)^2 + (-\epsilon^2 \Delta u + f'(u))(-\epsilon^2 \Delta u_{tt} + f''(u) u_t^2 + f'(u) u_{tt})$$
$$+ \eta \epsilon^2 (\nabla u_t)^2 + \eta \epsilon^2 \nabla u \cdot \nabla u_{tt} + \eta f'(u)(u_t)^2 + \eta f(u) u_{tt} d\boldsymbol{x}.$$

We then have

$$|R_1^n| = C\Delta t \int_{t^n}^{t^{n+1}} |r_{tt}| ds \leq C\Delta t \int_{t^n}^{t^{n+1}} (\|u_t\|_{H^2}^2 + \|u_t\|_{H^2} + \|u_{tt}\|_{H^2}) ds.$$

For the first term on the right-hand side of (3.21),

$$\left| \|\nabla \mu(u(t^{n+1}))\|^2 - \frac{r^{n+1}}{E(\bar{u}^{n+1})} \|\nabla \mu(\bar{u}^{n+1})\|^2 \right|$$
$$\leq \|\nabla \mu(u(t^{n+1}))\|^2 \left| 1 - \frac{r^{n+1}}{E(\bar{u}^{n+1})} \right| + \frac{r^{n+1}}{E(\bar{u}^{n+1})} \left| \|\nabla \mu(u(t^{n+1}))\|^2 - \|\nabla \mu(\bar{u}^{n+1})\|^2 \right| := K_1^n + K_2^n.$$

For K_1^n and K_2^n, it follows from (3.6), (3.5), (3.18), (3.19), $E(u) \geq -L_0 + 1 > 0$ and Theorem 2.1 that

$$\begin{aligned} K_1^n &\leq C\left|1 - \frac{r^{n+1}}{E(\bar{u}^{n+1})}\right| \\ &\leq C\left|\frac{r(t^{n+1})}{E(u(t^{n+1}))} - \frac{r^{n+1}}{E(u(t^{n+1}))}\right| + \left|\frac{r^{n+1}}{E(u(t^{n+1}))} - \frac{r^{n+1}}{E(\bar{u}^{n+1})}\right| \\ &\leq C(|e_r^{n+1}| + |E(u(t^{n+1})) - E(\bar{u}^{n+1})|), \end{aligned}$$

and

$$\begin{aligned} K_2^n &\leq C\|\nabla\mu(u(t^{n+1})) - \nabla\mu(\bar{u}^{n+1})\|\left(\|\nabla\mu(u(t^{n+1}))\| + \|\nabla\mu(\bar{u}^{n+1})\|\right) \\ &\leq C\bar{C}(\|\nabla\Delta^2\bar{e}^{n+1}\| + \|\nabla\Delta\bar{e}^{n+1}\|)(1 + \|\nabla\Delta^2\bar{u}^{n+1}\|) \\ &\leq C\bar{C}\|\nabla\Delta^2\bar{e}^{n+1}\|\|\nabla\Delta^2\bar{u}^{n+1}\| + C\bar{C}\|\nabla\Delta\bar{e}^{n+1}\|\|\nabla\Delta^2\bar{u}^{n+1}\| + C\bar{C}(\|\nabla\Delta^2\bar{e}^{n+1}\| + \|\nabla\Delta\bar{e}^{n+1}\|). \end{aligned}$$

Using the Cauchy–Schwarz inequality, we derive

$$\begin{aligned} \Delta t\sum_{q=1}^{n+1}\|\nabla\Delta^2\bar{e}^q\|\|\nabla\Delta\bar{u}^q\| &\leq (\Delta t\sum_{q=1}^{n+1}\|\nabla\Delta^2\bar{e}^q\|^2\Delta t\sum_{q=1}^{n+1}\|\nabla\Delta\bar{u}^q\|^2)^{1/2} \\ &\leq \bar{C}\sqrt{C_2(1+C_0^{2k+2})}\Delta t^k, \\ \Delta t\sum_{q=1}^{n+1}\|\nabla\Delta^2\bar{e}^q\|\|\nabla\Delta^2\bar{u}^q\| &\leq (\Delta t\sum_{q=1}^{n+1}\|\nabla\Delta^2\bar{e}^q\|^2\Delta t\sum_{q=1}^{n+1}\|\nabla\Delta^2\bar{u}^q\|^2)^{1/2} \\ &\leq \bar{C}\sqrt{C_2(1+C_0^{2k+2})}\Delta t^k. \end{aligned}$$

Next, we have

$$\begin{aligned} &|E(u(t^{n+1})) - E(\bar{u}^{n+1})| \\ \leq&\frac{1}{2}\|-\epsilon^2\Delta u(t^{n+1}) + f(u(t^{n+1}))\|\|\epsilon^2\Delta\bar{e}^{n+1} - (f(\bar{u}^{n+1}) - f(u(t^{n+1})))\| \\ &+ \frac{1}{2}\|-\epsilon^2\Delta\bar{u}^{n+1} + f(\bar{u}^{n+1})\|\|\epsilon^2\Delta\bar{e}^{n+1} - (f(\bar{u}^{n+1}) - f(u(t^{n+1})))\| \\ &+ \frac{\eta\epsilon^2}{2}(\|\nabla u(t^{n+1})\| + \|\nabla\bar{u}^{n+1}\|)\|\nabla u(t^{n+1}) - \nabla\bar{u}^{n+1}\| + \eta\|F(u(t^{n+1})) - F(\bar{u}^{n+1})\| \\ \leq&C(\|\Delta\bar{e}^{n+1}\| + \|\nabla\bar{e}^{n+1}\| + \|\bar{e}^{n+1}\|). \end{aligned}$$

Taking the sum of (3.21) over n from 0 to m, after combining the above estimates together, we obtain

$$\begin{aligned} |e_r^{m+1}| &\leq \Delta t\sum_{q=0}^{m}\left|\|\nabla\mu(u(t^{q+1}))\|^2 - \frac{r^{q+1}}{E(\bar{u}^{q+1})}\|\nabla\mu(\bar{u}^{q+1})\|^2\right| + \sum_{q=0}^{m}|T_1^q| \\ &\leq C\Delta t\sum_{q=0}^{m}|e_r^{q+1}| + C\Delta t\sum_{q=0}^{m}\|\bar{e}^{q+1}\|_{H^2} + C\Delta t\int_0^T(\|u_t\|_{H^2}^2 + \|u_t\|_{H^2} + \|u_{tt}\|_{H^2})ds \\ &\leq C\Delta t\sum_{q=0}^{m}|e_r^{q+1}| + C\bar{C}\sqrt{C_2(1+C_0^{2k+2})}\Delta t^k + C\Delta t. \end{aligned}$$

Using the Grönwall's inequality, we obtain

$$|e_r^{m+1}| \leq C\exp((1-C\Delta t)^{-1})\Delta t(\bar{C}\sqrt{C_2(1+C_0^{2k+2})}\Delta t^{k-1} + 1). \tag{3.22}$$

Thanks to (3.22), we can define C_0 and finish the proof virtually the same as **Step 3** of Theorem 3 in [19] under the condition

$$\Delta t \leq \frac{1}{1+C_0^{k+2}}, \quad 1 \leq k \leq 5. \tag{3.23}$$

Then we have $|1 - \xi^{m+1}| \leq C_0\Delta t$. This completes the induction process.

Finally, we can obtain $\|\bar{e}^{m+1}\|_{H^2}^2 + \|e^{m+1}\|_{H^2}^2 \leq C\Delta t^{2k}$ as follows.

From (3.19) and (2.2d), and noting the result in (3.3), we can conclude that

$$\left\|u^{m+1} - \bar{u}^{m+1}\right\|_{H^2} \leq \left|\eta_k^{m+1} - 1\right|\left\|\bar{u}^{m+1}\right\|_{H^2} \leq \bar{C}\left|\eta_k^{m+1} - 1\right| \leq \bar{C}C_0^{k+1}\Delta t^{k+1}. \tag{3.24}$$

Combining (3.24) with the conditions (3.4) and (3.23) on the time step Δt, we derive that

$$\begin{aligned} \left\|e^{m+1}\right\|_{H^2}^2 &\leq 2\left\|\bar{e}^{m+1}\right\|_{H^2}^2 + 2\left\|u^{m+1} - \bar{u}^{m+1}\right\|_{H^2}^2 \\ &\leq 2C_2\left(1 + C_0^{2(k+1)}\right)\Delta t^{2k} + 2\bar{C}^2C_0^{2(k+1)}\Delta t^{2(k+1)}, \end{aligned}$$

provided that $\Delta t < \frac{1}{1+2C_0^{k+2}}$. This completes the proof. □

Remark 3.2. Note that for the case $k = 1$, we employ $\eta_1^{n+1} = 1 - (1 - \xi^{n+1})^3$ purely for technical reasons. It is apparent that $\eta_1^{n+1} = 1 - (1 - \xi^{n+1})^2$ will ensure first-order accuracy.

4. Numerical simulations

In this section, we provide several numerical examples to verify the accuracy and stability of the proposed numerical schemes. The computational domain is defined as $\Omega = [0, L)^d$ $(d = 2, 3)$ with periodic boundary conditions. Unless otherwise specified, the mobility constant is set to $\mathcal{M} = 1$.

4.1. Fully discrete schemes

We observe that at each time step, the scheme (2.2a) reduces to solving the following coupled linear system

$$\begin{aligned} &\frac{\alpha_k \bar{u}^{n+1}}{\Delta t} - \mathcal{M}\Delta\bar{\mu}^{n+1} = g_1^n,\\ &\bar{\mu}^{n+1} + \epsilon^2\Delta\bar{\omega}^{n+1} = g_2^n,\\ &\bar{\omega}^{n+1} + \epsilon^2\Delta\bar{u}^{n+1} = g_3^n, \end{aligned} \tag{4.1}$$

with either periodic boundary conditions or homogeneous Neumann boundary conditions. In the above g_i^n $(i = 1, 2, 3)$ are known functions from the previous steps.

In the case of periodic boundary conditions, we can apply a Fourier-spectral method to the above system with unknowns being the Fourier-coefficients of the unknown functions so that the Fourier approximation of the above system reduces to a diagonal system. Thus the scheme (2.2) can be efficiently implemented using a Fourier-spectral method.

On the other hand, in the case of homogeneous Neumann boundary conditions, one can apply a Legendre-Spectral method to (4.1). Then, the corresponding coupled linear system can also be efficiently solved by using the method presented in [13].

4.2. Accuracy test

We set $d = 2$, $L = 2\pi$, and assume the exact solution is given by

$$u(x, y, t) = 0.25\cos(x)\cos(y)e^{-t}. \tag{4.2}$$

We use the Fourier-Galerkin method in space with 256 × 256 Fourier modes. Fig. 1 presents the errors at $T = 1$, measured in the H^2-norm for u and the L^∞-norm for $|1 - \xi|$ for the FCH equation, i.e., $\eta < 0$ with $\mathcal{M} = 0.005$, $\epsilon = 1$ and $\eta = -1$. It is evident that all schemes achieve the expected convergence rate in time. Similar results were observed for $\eta \geq 0$. For the sake of brevity, we do not report them here.

4.3. Phase separation

To simulate the coarsening dynamics, we consider sixth-order Cahn–Hilliard-type Eq. (1.1) in the domain $[0, 4\pi)^d$ $(d = 2, 3)$, with $\epsilon = 0.1$.

4.3.1. FCH equation

We first consider the 2D FCH equation to model the bilayer network structure. We set $\eta = -\epsilon^2$, and use 256 × 256 Fourier modes with the following initial condition:

$$u(x, y, t = 0) = 0.5 + 0.001\text{Rand}(x, y), \tag{4.3}$$

where $\text{Rand}(x, y)$ denotes the random values in $[-1, 1]^2$.

In Figs. 2(a)–2(b), we present the energy evolution profiles utilizing varying time step sizes for both implicit-explicit (IMEX) schemes and GSAV schemes. We observe that the GSAV schemes exhibit superior performance over the IMEX scheme, particularly at larger time steps. Furthermore, the original energy obtained by the GSAV schemes are consistently dissipative, whereas the energy of IMEX schemes blows up at larger time steps and exhibits an increase at certain times even at smaller time steps.

For subsequent simulations, we shall use the second-order GSAV scheme, unless specified otherwise.

Fig. 3 depicts the dynamics of phase separation with $\eta = -\epsilon^2$ and $\Delta t = 1 \times 10^{-3}$. The red areas represent the presence of amphiphilic polymers ($u = -1$), while the black regions indicate the solvent phase ($u = +1$). The narrow worm-like bilayers merge to form enclosed regions at around $t = 10$. Some interesting structures like Y-junctions and antennae are captured at $t = 50$ and $t = 100$, respectively. Eventually, the interface elongates and merges to form a network-like structure.

For the 3D case, we still set $\eta = -\epsilon^2$, $\Delta t = 1 \times 10^{-3}$ with the initial condition

$$u(x, y, z, t = 0) = 0.5 + 0.001\text{Rand}(x, y, z), \tag{4.4}$$

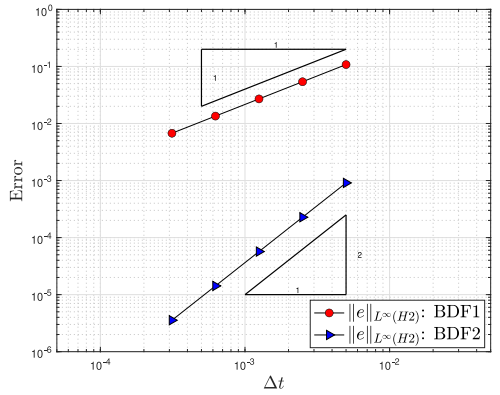

(a) BDF1 and BDF2 vs. errors of u

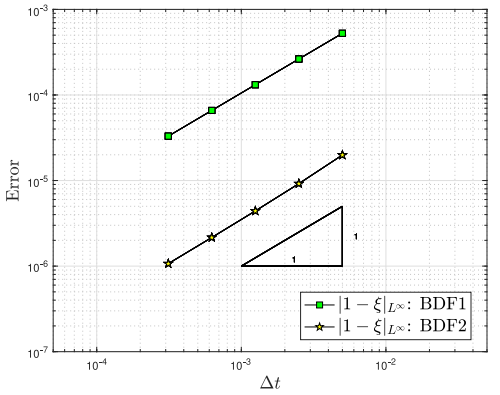

(b) BDF1 and BDF2 vs. errors of ξ

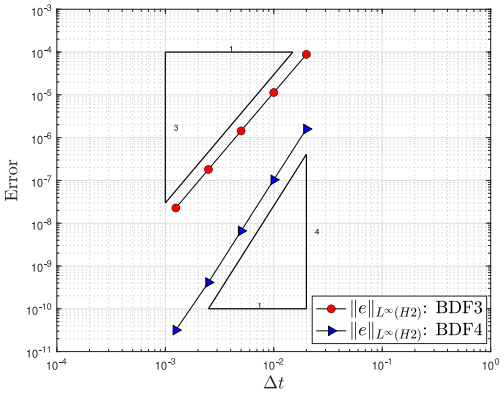

(c) BDF3 and BDF4 vs. errors of u

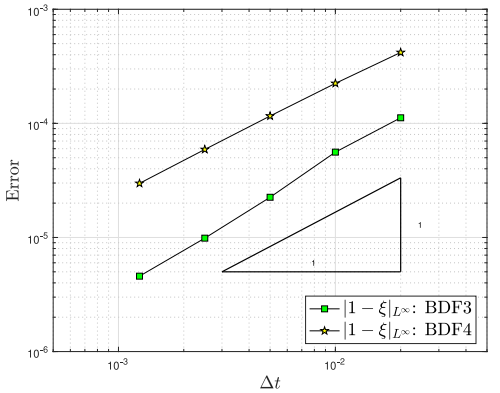

(d) BDF3 and BDF4 vs. errors of ξ

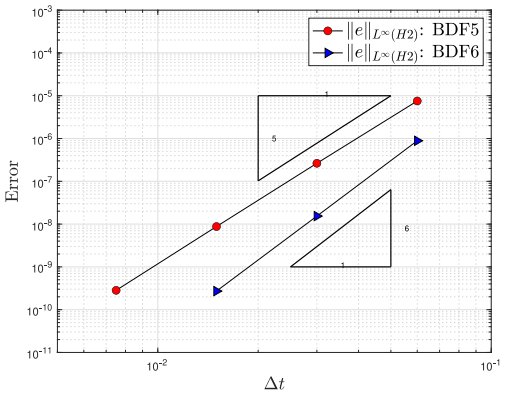

(e) BDF5 and BDF6 vs. errors of u

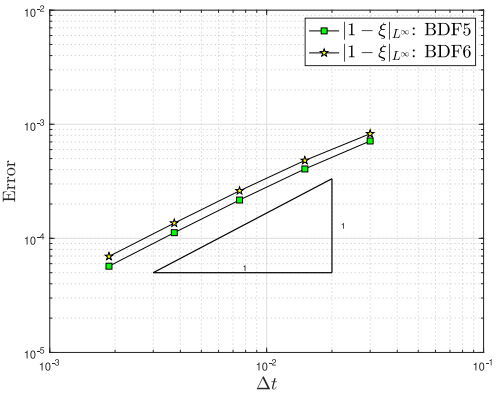

(f) BDF5 and BDF6 vs. errors of ξ

Fig. 1. Numerical convergence rate of schemes (2.2): convergence rate depicted by the triangle.

where Rand(x, y, z) denotes random values in $[-1, 1]^3$. In Fig. 4, we plot three iso-surface diagrams (above) and three slice diagrams (below) with yellow and black regions correspond to the level sets $u = 0$ and $u = 0.2$, respectively. We observed similar phase separation behaviors to those observed in the 2D case. These results are consistent with those reported in [28–31].

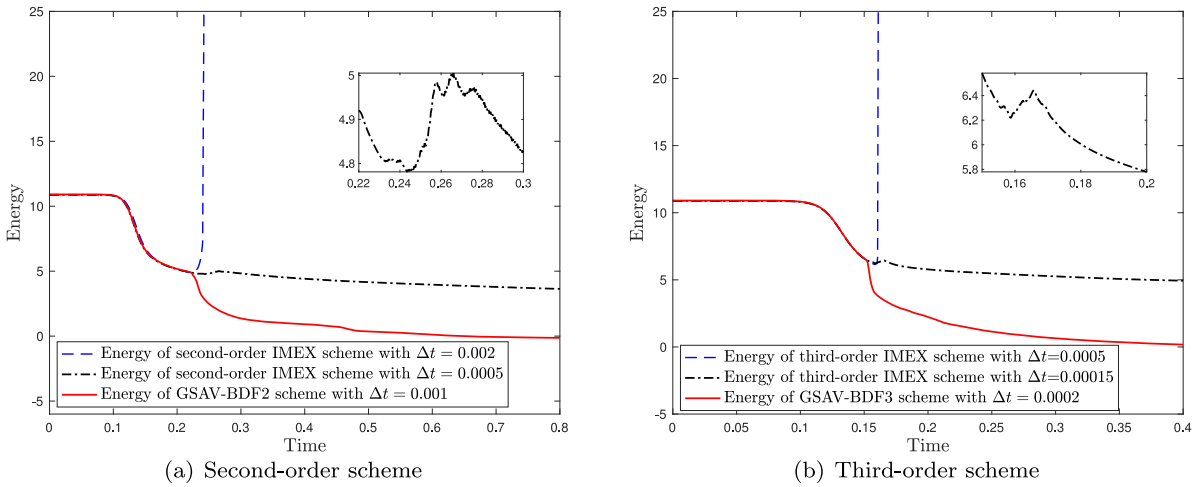

Fig. 2. Comparison of energy evolution curves for both the IMEX scheme and GSAV-BDFk scheme with different time steps.

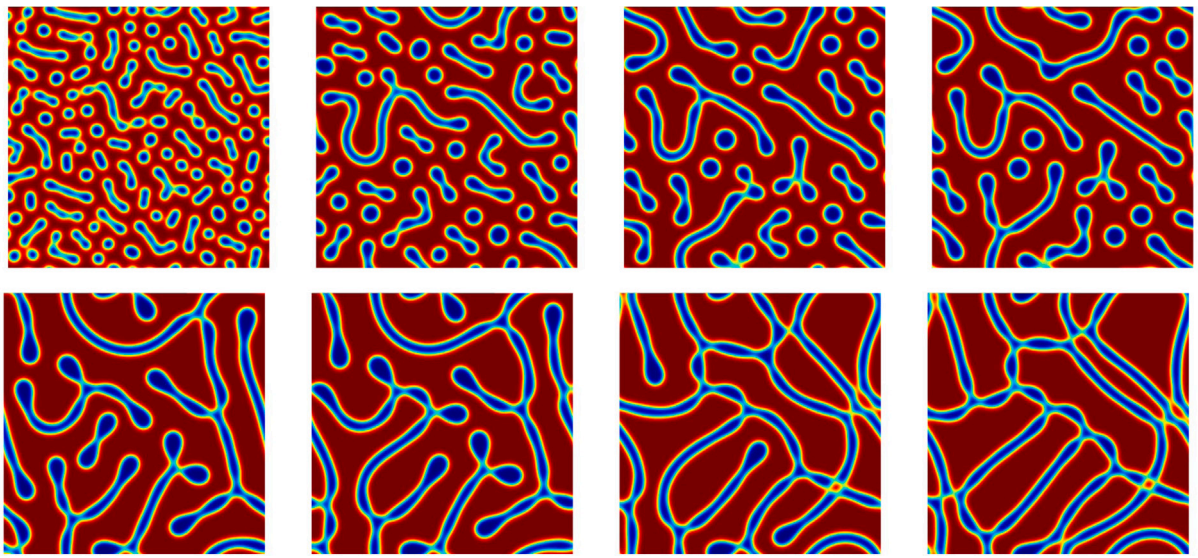

Fig. 3. The phase variable u is simulated using the specified initial condition described in (4.3) with $\eta = -\epsilon^2$. Snapshots for the simulation of 2D phase separation for FCH equation are captured at various times $t = 1,\ 10,\ 50,\ 100,\ 500,\ 1000,\ 3000$ and 5000.

4.3.2. CHW equation

In this example, we use the initial condition in (4.3) to simulate the Cahn–Hilliard equation with Willmore-regularization, i.e., $\eta > 0$. More precisely, we set $\eta = \epsilon$ and investigate the coarsening process using 256×256 Fourier modes with a time step of $\Delta t = 1 \times 10^{-3}$. In Fig. 5, we present snapshots of the phase variable u are captured at $t = 2,\ 10,\ 30,\ 50,\ 200,\ 500,\ 1000$ and 5000 which clearly exhibit the coarsening process.

4.4. A benchmark problem

We consider a benchmark problem [32] with the initial condition

$$u(x, y, t = 0) = 2\exp(\sin x + \sin y - 2) + 2.2\exp(-\sin x - \sin y - 2) - 1, \tag{4.5}$$

and the following parameters

$$\epsilon = 0.18, \quad \eta = -0.0324, \quad d = 2, \quad L = 2\pi.$$

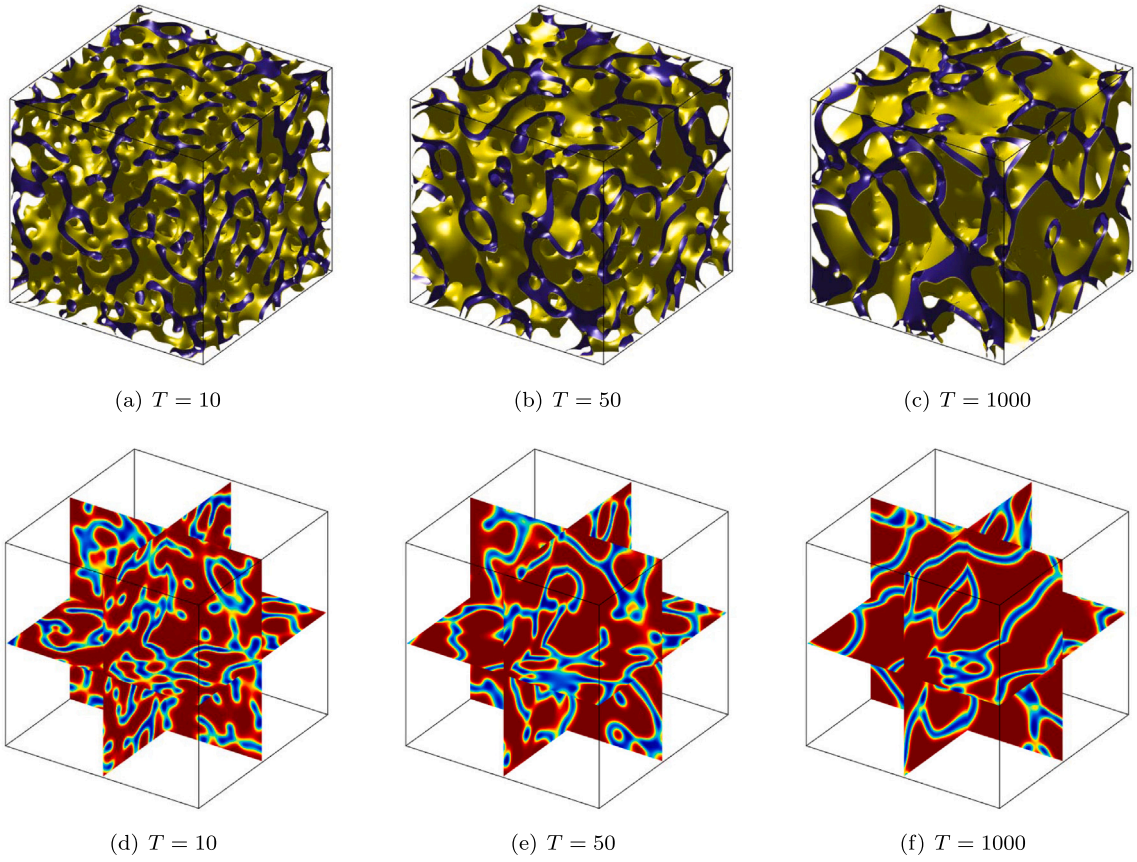

Fig. 4. Iso-surface diagrams (above) and slice diagrams (below) of 3D phase separation for FCH equation are captured at various times $t = 10,\ 50$ and 100.

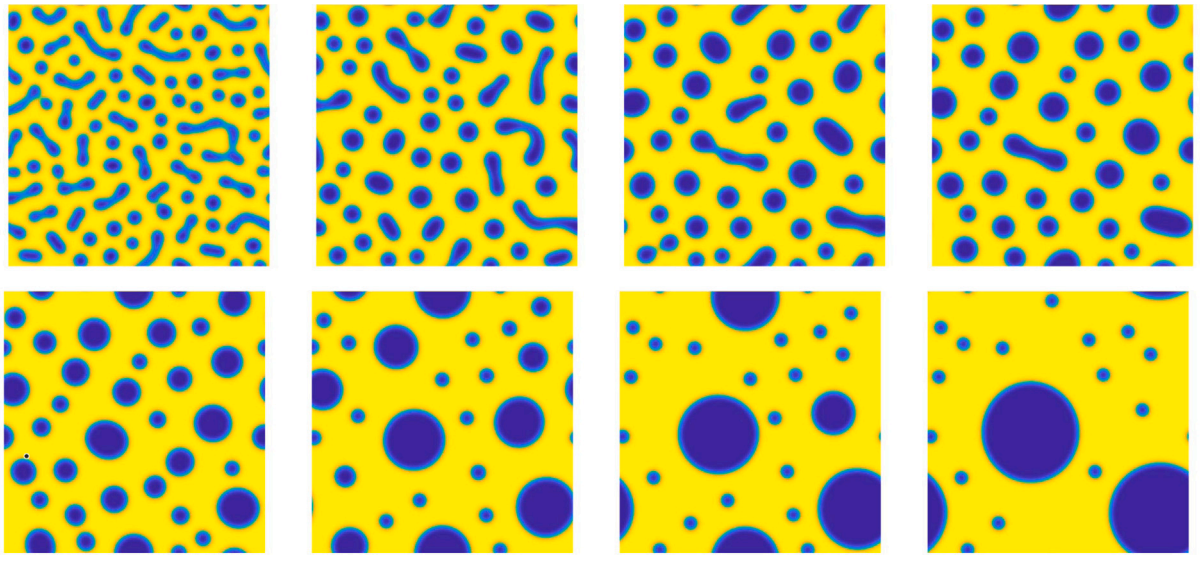

Fig. 5. The phase variable u is simulated using the specified initial condition described in (4.3) with $\eta = \epsilon$. Snapshots for the simulation of coarsening process for CHW equation are captured at various times $t = 2,\ 10,\ 30,\ 50,\ 100,\ 500,\ 2000$ and 5000.

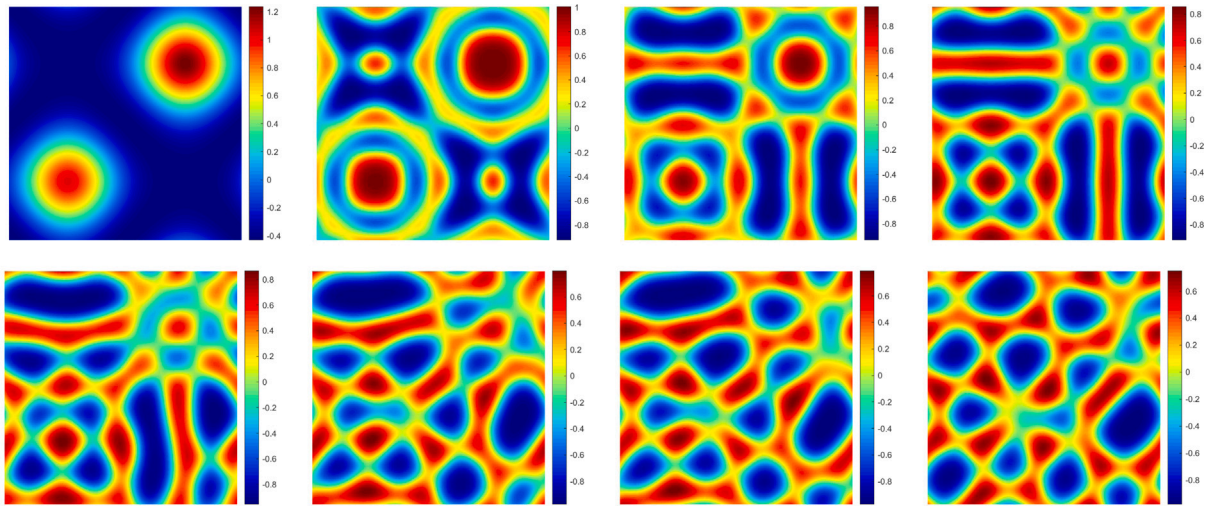

Fig. 6. The phase variable u is simulated using the specified initial condition described in (4.5) with $\eta = -0.0324$. Snapshots for the simulation of a benchmark problem are captured at various times $t = 0,\ 1,\ 5,\ 20,\ 400,\ 500,\ 600$ and 1000.

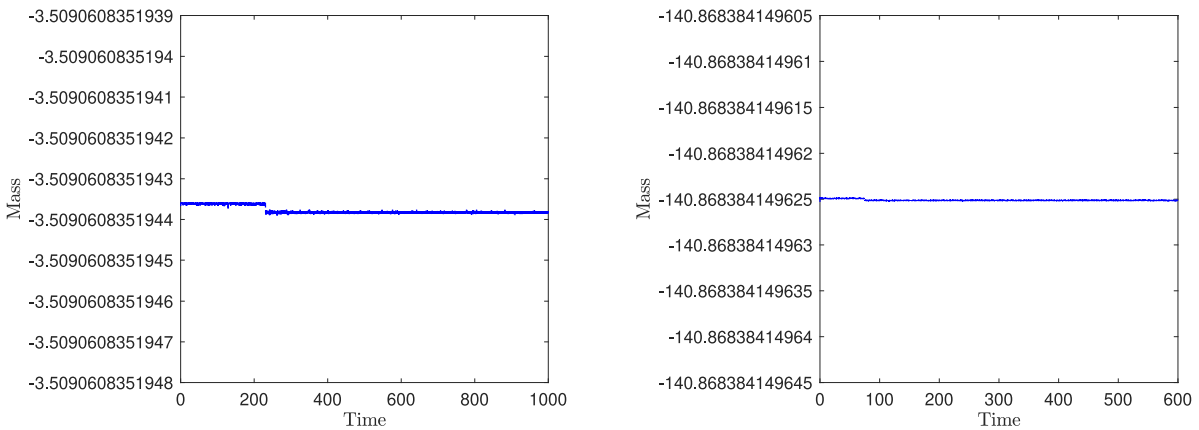

(a) Initial conditions from (4.5) (b) Initial conditions from (4.6)

Fig. 7. Evolutions of mass of u in the sixth-order Cahn–Hilliard-type equation with different initial conditions.

We use 128×128 Fourier modes in space and $\Delta t = 5 \times 10^{-4}$. In Fig. 6, we present snapshots of the phase variable to show the formation of the anticipated network structure in the amphiphilic materials, which is consistent with the results reported in [15,32]. We observe that the mass of u is almost conserved, as shown in Fig. 7(a).

4.5. Meandering instability

To simulate the meandering instability, we take the initial condition as follows:

$$u(x, y, t = 0) = \begin{cases} -1, & x > \sin(y) + 2\pi + 0.34, \\ -1, & x < \sin(y) + 2\pi - 0.34, \\ 1, & \text{otherwise.} \end{cases} \tag{4.6}$$

The parameters are given by:

$$\epsilon = 0.1, \quad \eta = -0.2, \quad d = 2, \quad L = 4\pi. \tag{4.7}$$

Note that the initial condition above is discontinuous, so we use a smoothed approximation as described in [2,16] to serve as the actual discrete initial condition.

We use 256×256 Fourier modes in space and $\Delta t = 1 \times 10^{-4}$. Fig. 7(b) demonstrates that the mass of u is almost conserved. The simulation results depicted in Fig. 8 illustrate the stretching of the initial shape and the emergence of meandering instability.

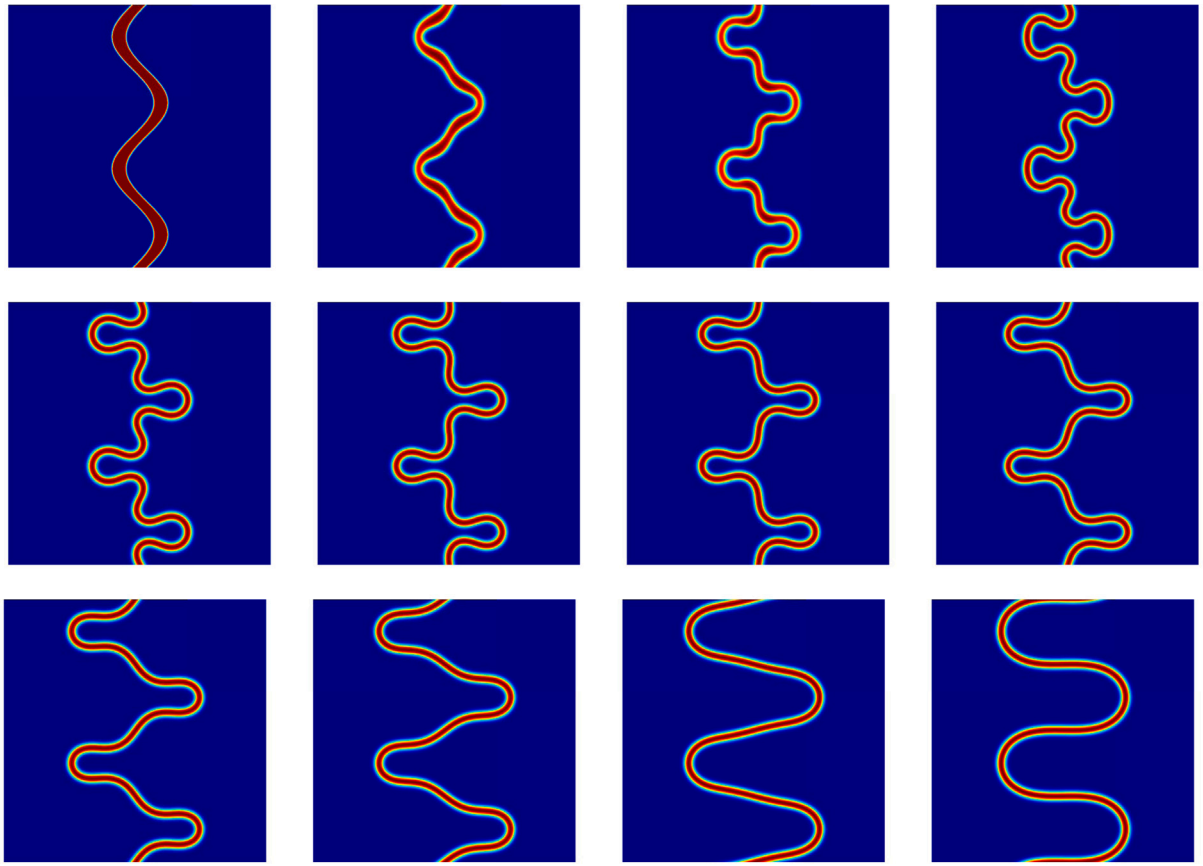

Fig. 8. The phase variable u is simulated using the specified initial condition described in (4.6) with $\eta = -0.2$. Snapshots for the simulation of meandering instability are captured at various times $t = 0,\ 10,\ 15,\ 20,\ 50,\ 100,\ 150,\ 200,\ 300,\ 400,\ 600$ and 1000.

Furthermore, it is noticeable that the configuration of the curve gradually evolves in the later times, with a progressive elongation primarily in the horizontal direction.

4.6. Pearling instability in annuli

In the last example, we consider a more complex FCH model [2] with the free energy

$$E(u) = \int_{\Omega} \left[\frac{1}{2} \left| -\epsilon^2 \Delta u + f(u) \right|^2 + \left(\eta_1 \frac{\epsilon^2}{2} |\nabla u|^2 + \eta_2 F(u) \right) \right] d\boldsymbol{x}. \tag{4.8}$$

Here, $\eta_1 < 0$ and $\eta_2 \in \mathbb{R}$ are two small parameters associated with the properties of amphiphilic materials. It reduces to the original free energy (1.1) $\eta_1 = \eta_2$.

The H^{-1} gradient flow associated with (4.8) is as follows:

$$\begin{cases} \partial_t u = \mathcal{M} \Delta \mu, & t > 0,\ \boldsymbol{x} \in \Omega, \\ \mu = -\epsilon^2 \Delta \omega + f'(u)\omega + \eta_1 \omega - (\eta_1 - \eta_2) f(u), & t > 0,\ \boldsymbol{x} \in \Omega, \\ \omega = -\epsilon^2 \Delta u + f(u), & t > 0,\ \boldsymbol{x} \in \Omega, \end{cases} \tag{4.9}$$

where

$$F(u) = \frac{1}{4}(u+1)^2(u-1)^2 + \frac{1}{24}(u+1)^2(u-2).$$

It is clear that the scheme (2.2) can also be applied to the above system.

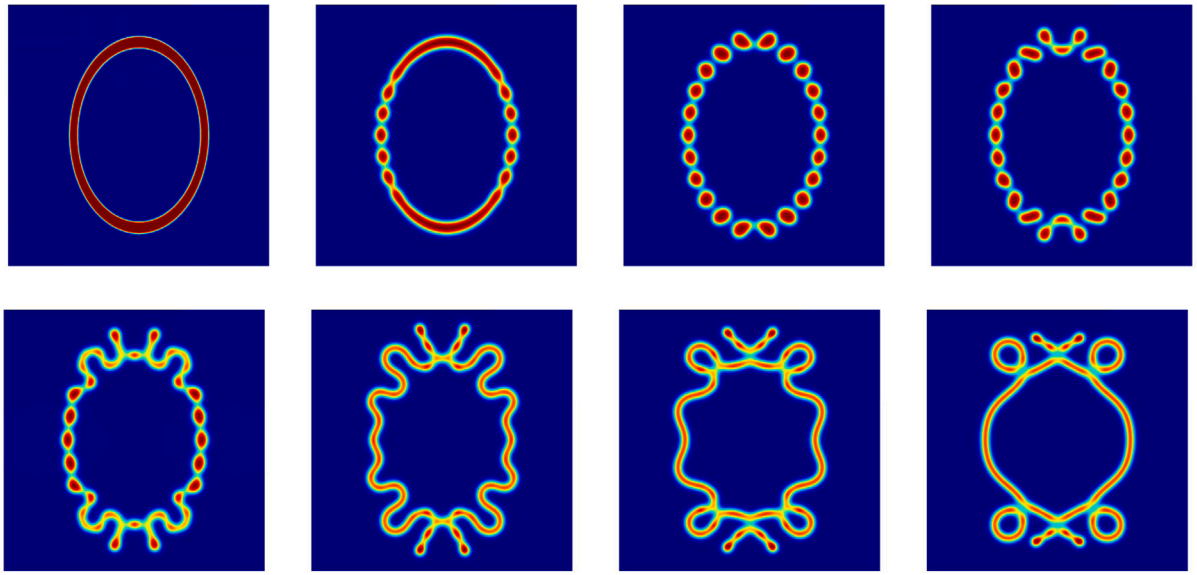

Fig. 9. The phase variable u is simulated using the GSAV-BDF2 scheme, starting from the initial condition specified in (4.10). Snapshots of the simulated phase variable u are captured at various times $t = 0,\ 2,\ 10,\ 15,\ 20,\ 30,\ 60$ and 122.

4.6.1. A ring-shaped ellipse

We consider the discontinuous initial condition

$$u(x, y, t = 0) = \begin{cases} -1, & f(x, y) > L/4 + 0.2, \\ -1, & f(x, y) < L/4 - 0.2, \\ 1, & \text{otherwise}, \end{cases} \tag{4.10}$$

where $f(x, y) = \sqrt{(x - L/2)^2 + 0.5(y - L/2)^2}$, and use a smoothed approximation as the discrete initial condition.

The parameters are as follows

$$\epsilon = 0.1, \quad \eta_1 = -0.145, \quad \eta_2 = -0.2, \quad d = 2, \quad L = 4\pi. \tag{4.11}$$

Fig. 9 illustrates the snapshots of the phase variable obtained with 256×256 Fourier modes in space and $\Delta t = 5.0 \times 10^{-4}$. We observe that, at time $T = 2$, the pearling bifurcation becomes noticeable, with the initial perturbation appearing at the midpoint of the minor axis of the elliptical ring, likely due to the relatively thinner bilayer in these areas. These budding pearls merge into a linear sequence at $T = 20$, leading to a meandering instability.

4.6.2. A ring-shaped circular

We simulate phases undergoing pearling instabilities, with the initial condition being

$$u(x, y, t = 0) = 2\cosh^{-1}\left(\frac{\sqrt{(x - 2\pi)^2 + (y - 2\pi)^2} - \pi}{q}\right) - 1, \tag{4.12}$$

which is a smoothed circular ring with interfacial width q. We use the parameters in (4.11), $\epsilon = 0.1$, $\eta_1 = \eta_2 = -0.2$, $d = 2$, $L = 4\pi$, and use 256×256 Fourier modes in space and $\Delta t = 1.0 \times 10^{-3}$. To investigate the effect of varying thickness on the final numerical results, we select different values for the parameter q, specifically $q = 0.14, 0.15$, and 0.20. The numerical results can be found in Figs. 10, 11 and 12. A sharper initial interface leads to rapid interfacial relaxation, which in turn accelerates the onset of pearling bifurcation caused by instabilities due to high curvature. By comparing these figures, we observe that different shapes emerge depending on the initial interface width q, with the pearling bifurcation occurring earlier when the thickness of the initial interface is smaller. The simulation results are in agreement with the transmission electron microscopy images of diblock copolymers presented in [33] and align with the numerical simulations shown in [2,34,35].

5. Concluding remarks

We constructed in this paper a class of high-order implicit-explicit (IMEX) schemes based on the GSAV approach for sixth-order Cahn–Hilliard-type equations which include, as specific examples, Cahn–Hilliard equation with Willmore regularization and functionalized Cahn–Hilliard equation. The proposed schemes are linear and only require solving one elliptic equation with constant

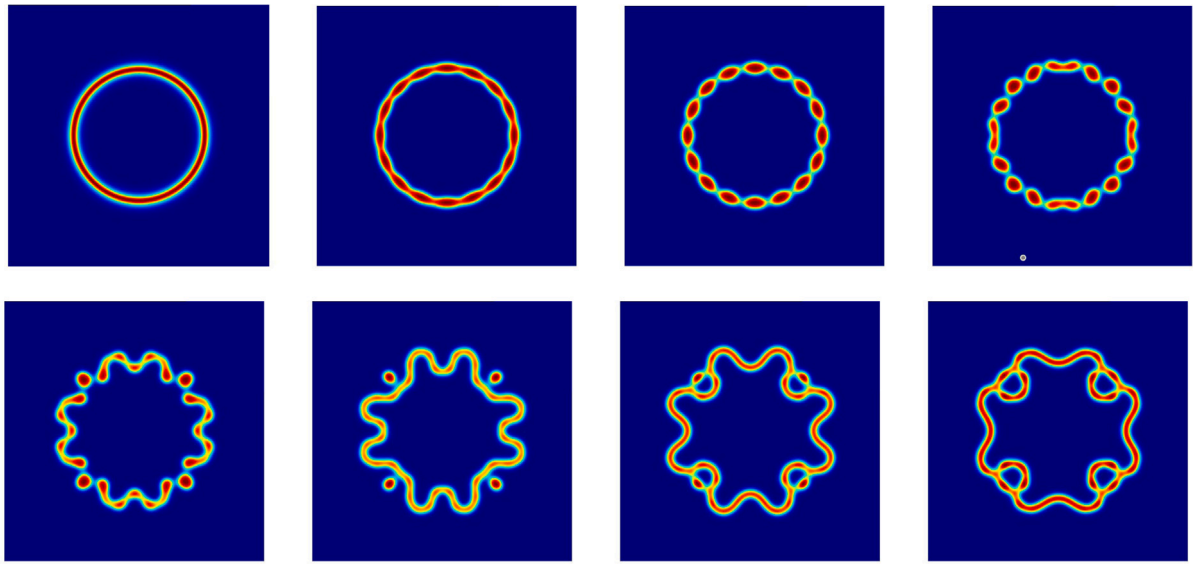

Fig. 10. The phase variable u is simulated using the GSAV-BDF2 scheme, starting from the initial condition specified in (4.12) with $q = 0.14$. Snapshots of the simulated phase variable u are captured at various times $t = 0,\ 9,\ 10,\ 22,\ 25,\ 30,\ 83$ and 100.

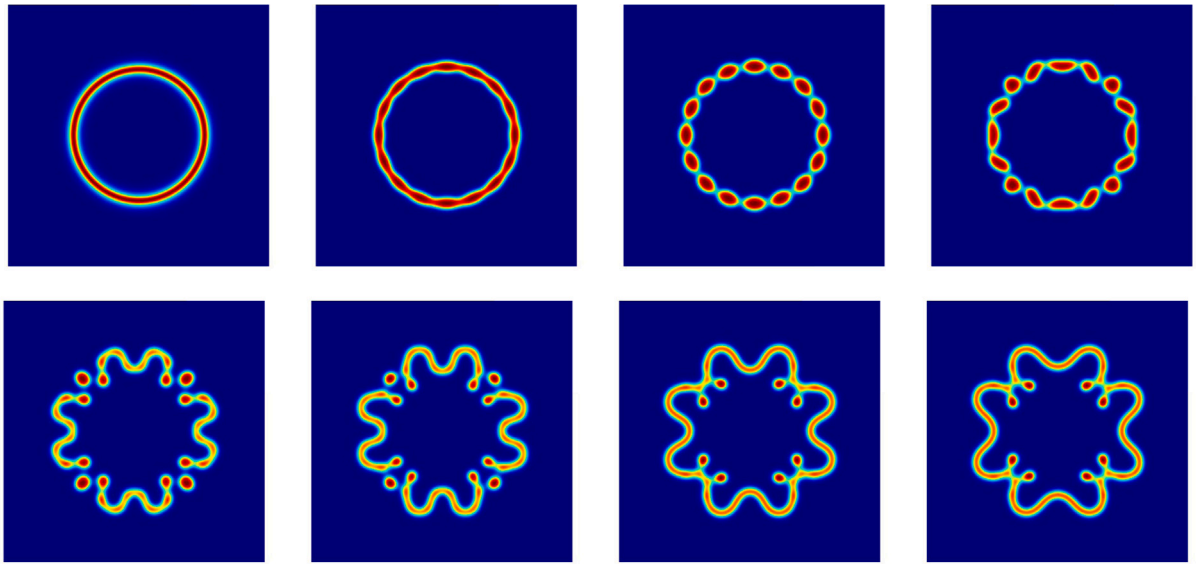

Fig. 11. The phase variable u is simulated using the GSAV-BDF2 scheme, starting from the initial condition specified in (4.12) with $q = 0.15$. Snapshots of the simulated phase variable u are captured at various times $t = 0,\ 13,\ 15,\ 24,\ 30,\ 34,\ 70$ and 100.

coefficients at each time step, dissipate a modified energy unconditionally, and their numerical solutions are uniformly bounded in $l^{\infty}(0,T;H^2(\Omega))$. We also carried out a rigorous error analysis using a delicate induction process, and derived optimal error estimates up to fifth-order. To the best of our knowledge, these are the first error estimates for higher-order numerical schemes for sixth-order Cahn–Hilliard-type equations.

We presented numerical evidence to validate the stability and accuracy of the proposed schemes which are shown to be superior to the standard IMEX schemes. We also presented ample numerical experiments to simulate various interesting dynamics processes generated by the Cahn–Hilliard equation with Willmore regularization and functionalized Cahn–Hilliard equation.

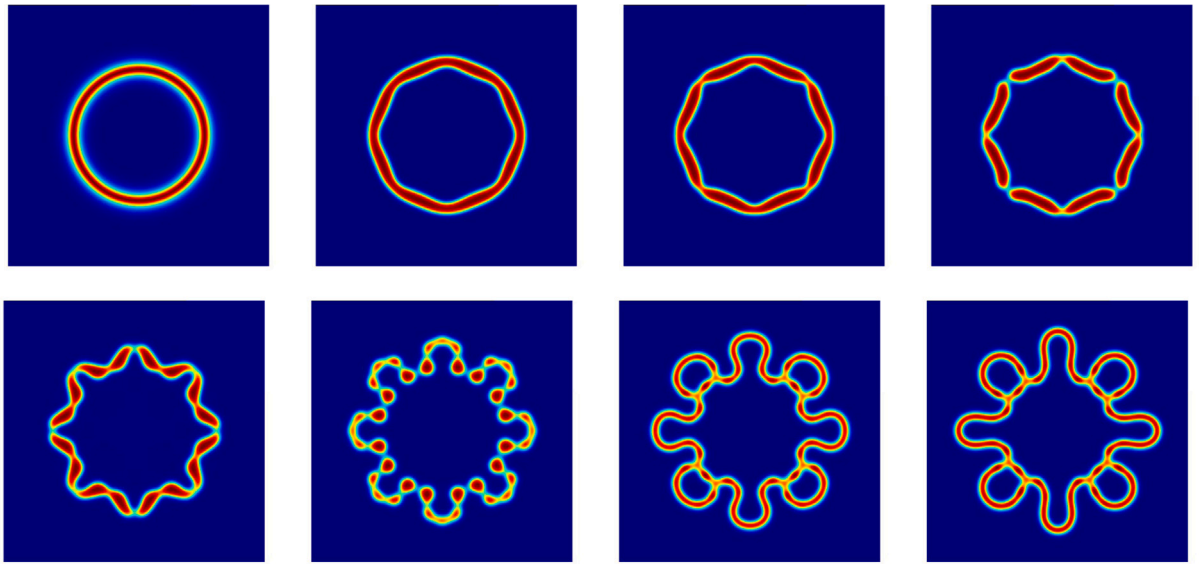

Fig. 12. The phase variable u is simulated using the GSAV-BDF2 scheme, starting from the initial condition specified in (4.12) with $q = 0.20$. Snapshots of the simulated phase variable u are captured at various times $t = 0,\ 49,\ 50,\ 51,\ 55,\ 60,\ 70$ and 100.

CRediT authorship contribution statement

Nan Zheng: Writing – original draft, Visualization, Software, Methodology, Investigation, Formal analysis, Conceptualization. **Jie Shen:** Writing – review & editing, Validation, Supervision, Resources, Project administration, Conceptualization.

Declaration of competing interest

The authors declare that they have no known competing financial interests or personal relationships that could have appeared to influence the work reported in this paper.

Acknowledgments

J. Shen is supported in part by NSFC, China grants 12371409 and W2431008. N. Zheng is supported the Hong Kong Polytechnic University Postdoctoral Research Fund 1-W22P.

Appendix. Bounds for the terms I_j $(j = 1, \dots, 6)$ in (3.9)

We now bound the terms I_j $(j = 1, \dots, 6)$ in (3.9) as follows. Firstly, using Hölder inequality, we obtain

$$\begin{aligned} I_1 \le & \frac{\|\Delta A_k(u^n) - \Delta A_k(\bar{u}^n)\|^2}{2\Delta t} + \frac{\Delta t}{2}\|\Delta\bar{e}^{n+1} - \tau_k\Delta\bar{e}^n\|^2 \\ \le & CC_0^{2k+2}\Delta t^{2k+1} + \Delta t(\|\Delta\bar{e}^{n+1}\|^2 + \|\Delta\bar{e}^n\|^2), \end{aligned} \tag{A.1}$$

and

$$\begin{aligned} I_2 = & \epsilon^4\Delta t(\nabla\Delta^2\bar{e}^{n+1}, \tau_k\nabla\Delta^2\bar{e}^n) \\ \le & \frac{\epsilon^4\Delta t}{2}\|\nabla\Delta^2\bar{e}^{n+1}\|^2 + \frac{\epsilon^4\Delta t}{2}\tau_k^2\|\nabla\Delta^2\bar{e}^n\|^2. \end{aligned} \tag{A.2}$$

It follows from (3.8) that

$$\|\nabla R_k\|^2 \le C\Delta t^{2k+1}\int_{t^{n+1-k}}^{t^{n+1}} \|\nabla\frac{\partial^{k+1}u}{\partial t^{k+1}}(s)\|^2 ds,$$

then we can derive

$$\begin{aligned} I_3 \le & \frac{C}{\Delta t}\|\nabla R_k^n\|^2 + \frac{\epsilon^2\Delta t}{4}\| - \nabla\Delta\bar{e}^{n+1} + \tau_k\nabla\Delta\bar{e}^n\|^2 \\ \le & C\Delta t^{2k}\int_{t^{n+1-k}}^{t^{n+1}} \|\nabla\frac{\partial^{k+1}u}{\partial t^{k+1}}(s)\|^2 ds + \frac{\epsilon^2\Delta t}{2}(\|\nabla\Delta\bar{e}^{n+1}\|^2 + \|\nabla\Delta\bar{e}^n\|^2). \end{aligned} \tag{A.3}$$

Next we estimate the terms I_4, I_5 and I_6. To this end, we need to bound $Q_i^n,\ i = 1, 2, 3$.

By the definition of Q_1^n, we have

$$\|\Delta Q_1^n\| \le \|\Delta^2 f(B_k(u(t^n))) - \Delta^2 f(B_k(\bar{u}^n))\| + \|\Delta^2 f(u(t^{n+1})) - \Delta^2 f(B_k(u(t^n)))\|.$$

Using the identities

$$\Delta f(u) = f'(u)\Delta u + f''(u)|\nabla u|^2, \tag{A.4}$$

and

$$\begin{aligned}\Delta^2 f(u) =& 6|\nabla u|^2\Delta u + f''(u)(\Delta u)^2 + f'(u)\Delta^2 u + 2f''(u)\nabla u\cdot\nabla\Delta u\\ &+ 6\Delta u|\nabla u|^2 + f''(u)\Delta|\nabla u|^2 + 12\nabla u\cdot\nabla\Delta u,\end{aligned}$$

we can estimate ΔQ_1^n term by term.

For simplicity, we only estimate the first two terms. Thanks to (3.5) and (3.6), we obtain by Hölder's inequality and Sobolev embedding that

$$\begin{aligned}&6\||\nabla B_k(u(t^n))|^2\Delta B_k(u(t^n)) - |\nabla B_k(\bar{u}^n)|^2\Delta B_k(\bar{u}^n)\|\\ =&6\|\left(|\nabla B_k(u(t^n))| + |\nabla B_k(\bar{u}^n)|\right)\nabla B_k(\bar{e}^n)\Delta B_k(u(t^n))\| + 6\||\nabla B_k(\bar{u}^n)|^2\Delta B_k(\bar{e}^n)\|\\ \le& C\|\nabla B_k(u(t^n)) + \nabla B_k(\bar{u}^n)\|_{L^6}\|\nabla B_k(\bar{e}^n)\|_{L^6}\|\Delta B_k(u(t^n))\|_{L^6}\\ &+ C\||\nabla B_k(\bar{u}^n)|^2\|_{L^3}\|\Delta B_k(\bar{e}^n)\|_{L^6}\\ \le& C\|B_k(u(t^n)) + B_k(\bar{u}^n)\|_{H^2}\|\nabla B_k(\bar{e}^n)\|_{H^1}\|B_k(u(t^n))\|_{H^3}\\ &+ C\|B_k(\bar{u}^n)\|_{H^2}\|\Delta B_k(\bar{e}^n)\|_{H^1}\\ \le& C(\|\nabla B_k(\bar{e}^n)\| + \|\Delta B_k(\bar{e}^n)\| + \|\nabla\Delta B_k(\bar{e}^n)\|).\end{aligned}$$

Similarly, we can obtain

$$\begin{aligned}&\|f''(B_k(u(t^n)))(\Delta B_k(u(t^n)))^2 - f''(B_k(\bar{u}^n))(\Delta B_k(\bar{u}^n))^2\|\\ =&\|B_k(\bar{e}^n)(\Delta B_k(u(t^n)))^2\| + \|(\Delta B_k(u(t^n)) + \Delta B_k(\bar{u}^n))\Delta B_k(\bar{e}^n)\|\\ \le& C\|B_k(\bar{e}^n)\|_{L^6}\|(\Delta B_k(u(t^n)))^2\|_{L^3} + C\|(\nabla B_k(u(t^n)) + \nabla B_k(\bar{u}^n))\nabla\Delta B_k(\bar{e}^n)\|\\ \le& C\|B_k(\bar{e}^n)\|_{L^6}\|\Delta B_k(u(t^n))\|_{L^6}^2 + C\|\nabla B_k(u(t^n)) + \nabla B_k(\bar{u}^n)\|_{L^6}\|\nabla\Delta B_k(\bar{e}^n)\|_{L^3}\\ \le& C\|B_k(\bar{e}^n)\|_{H^1}\|\Delta B_k(u(t^n))\|_{H^1}^2 + C\|\nabla B_k(u(t^n)) + \nabla B_k(\bar{u}^n)\|_{H^1}\|\nabla\Delta B_k(\bar{e}^n)\|_{H^1}\\ \le& C(\|B_k(\bar{e}^n)\| + \|\nabla B_k(\bar{e}^n)\| + \|\Delta B_k(\bar{e}^n)\| + \|\nabla\Delta B_k(\bar{e}^n)\| + \|\Delta^2 B_k(\bar{e}^n)\|).\end{aligned}$$

Other terms in ΔQ_1^n can be bounded similarly, and we can obtain

$$\begin{aligned}\|\Delta Q_1^n\| \le& C\left(\|B_k(\bar{e}^n)\| + \|\nabla B_k(\bar{e}^n)\| + \|\Delta B_k(\bar{e}^n)\| + \|\nabla\Delta B_k(\bar{e}^n)\| + \|\Delta^2 B_k(\bar{e}^n)\|\right)\\ &+ \left(\Delta t\int_{t^{n+1-k}}^{t^{n+1}}\|\frac{\partial^k u}{\partial t^k}(s)\|_{H^4}^2 ds\right)^{1/2},\end{aligned}$$

which implies that

$$\begin{aligned}I_4 \le& \frac{\epsilon^2}{2}\Delta t(\|\Delta Q_1^n\|^2 + \|\Delta^2\bar{e}^{n+1} - \tau_k\Delta^2\bar{e}^n\|^2)\\ \le& \frac{\epsilon^2}{2}\Delta t(\|\Delta Q_1^n\|^2 + 2\|\Delta^2\bar{e}^{n+1}\|^2 + 2\|\Delta^2\bar{e}^n\|^2)\\ \le& C\Delta t\left(\|B_k(\bar{e}^n)\|^2 + \|\nabla B_k(\bar{e}^n)\|^2 + \|\Delta B_k(\bar{e}^n)\|^2 + \|\nabla\Delta B_k(\bar{e}^n)\|^2 + \|\Delta^2 B_k(\bar{e}^n)\|^2\right)\\ &+ C\Delta t^{2k}\int_{t^{n+1-k}}^{t^{n+1}}\|\frac{\partial^k u}{\partial t^k}(s)\|_{H^4}^2 ds + \epsilon^2\Delta t(\|\Delta^2\bar{e}^{n+1}\|^2 + \|\Delta^2\bar{e}^n\|^2).\end{aligned} \tag{A.5}$$

For ΔQ_2^n, we have

$$\begin{aligned}\|\Delta Q_2^n\| \le& \frac{1}{\epsilon^2}\|\Delta(f'(B_k(\bar{u}^n))B_k(\bar{\omega}^n)) - \Delta(f'(B_k(u(t^n)))B_k(\bar{\omega}^n))\|\\ &+\frac{1}{\epsilon^2}\|\Delta(f'(B_k(u(t^n)))B_k(\bar{\omega}^n)) - \Delta(f'(B_k(u(t^n)))B_k(\omega(t^n)))\|\\ &+\frac{1}{\epsilon^2}\|\Delta(f'(B_k(u(t^n)))B_k(\omega(t^n))) - \Delta(f'(B_k(u(t^{n+1})))B_k(\omega(t^n)))\|\\ &+\frac{1}{\epsilon^2}\|\Delta(f'(B_k(u(t^{n+1})))B_k(\omega(t^n))) - \Delta(f'(u(t^{n+1}))\omega(t^{n+1}))\|.\end{aligned} \tag{A.6}$$

We derive from the third equation of (2.2a) that

$$\begin{aligned}
&\frac{1}{\epsilon^2}\left\|\left(\Delta f'(B_k(\bar{u}^n)) - \Delta f'(B_k(u(t^n)))\right) B_k(\bar{\omega}^n)\right\| \\
\le& \left\|\nabla B_k(\bar{u}^n)\right\|_{L^6}\left\|\nabla\Delta f'(B_k(\bar{u}^n)) - \Delta f'(B_k(u(t^n)))\right\|_{L^3} \\
&+ \frac{1}{\epsilon^2}\left\|f(B_k(\bar{u}^n))\right\|_{L^\infty}\left\|\Delta f'(B_k(\bar{u}^n)) - \Delta f'(B_k(u(t^n)))\right\| \\
\le& \left\|\nabla\Delta f'(B_k(\bar{u}^n)) - \nabla\Delta f'(B_k(u(t^n)))\right\|_{H^1} + \left\|\Delta f'(B_k(\bar{u}^n)) - \Delta f'(B_k(u(t^n)))\right\| \\
\le& C(\|B_k(\bar{e}^n)\| + \|\nabla B_k(\bar{e}^n)\| + \|\Delta B_k(\bar{e}^n)\| + \|\nabla\Delta B_k(\bar{e}^n)\| + \|\Delta^2 B_k(\bar{e}^n)\|).
\end{aligned} \tag{A.7}$$

Using (A.4) and the identity

$$\Delta(fg) = f\Delta g + g\Delta f + 2\nabla f\cdot\nabla g,$$

other terms on the right-hand side of (A.6) can be estimated similarly to obtain

$$\begin{aligned}
\|\Delta Q_2^n\| \le& C\left(\|B_k(\bar{e}^n)\| + \|\nabla B_k(\bar{e}^n)\| + \|\Delta B_k(\bar{e}^n)\| + \|\nabla\Delta B_k(\bar{e}^n)\| + \|\Delta^2 B_k(\bar{e}^n)\|\right) \\
&+ C\Delta t^{k-1}(\Delta t\int_{t^{n+1-k}}^{t^{n+1}}\|\frac{\partial^k u}{\partial t^k}(s)\|_{H^4}^2 ds)^{1/2}.
\end{aligned}$$

For ΔQ_3^n, we have

$$\begin{aligned}
\|\Delta Q_3^n\| \le& \eta\|-\Delta^2 B_k(\bar{e}^n) + \frac{1}{\epsilon^2}\left(\Delta f(B_k(\bar{u}^n)) - \Delta f(B_k(u(t^n)))\right)\| \\
&+ \eta\|(-\Delta^2 B_k(u(t^n)) + \Delta^2 B_k(u(t^{n+1})))\| \\
&+ \frac{\eta}{\epsilon^2}\|\left(\Delta f(B_k(u(t^n))) - \Delta f(B_k(u(t^{n+1})))\right)\| \\
\le& \eta\|-\Delta^2 B_k(\bar{e}^n)\| + \frac{1}{\epsilon^2}\|\Delta f(B_k(\bar{u}^n)) - \Delta f(B_k(u(t^n)))\| \\
&+ \eta\|-\Delta^2 B_k(u(t^n)) + \Delta^2 B_k(u(t^{n+1}))\| \\
&+ \frac{\eta}{\epsilon^2}\|\Delta f(B_k(u(t^n))) - \Delta f(B_k(u(t^{n+1})))\| \\
\le& C\left(\|B_k(\bar{e}^n)\| + \|\nabla B_k(\bar{e}^n)\| + \|\Delta B_k(\bar{e}^n)\| + C\|\Delta^2 B_k(\bar{e}^n)\|\right) \\
&+ C\Delta t^{k-1}\left(\Delta t\int_{t^{n+1-k}}^{t^{n+1}}\|\frac{\partial^k u}{\partial t^k}(s)\|_{H^4}^2 ds\right)^{1/2}.
\end{aligned}$$

Similarly, we can bound the last two items on the right-hand side of (3.9) to get

$$\begin{aligned}
I_5 + I_6 \le& \frac{\epsilon^2}{2}\Delta t(\|\Delta Q_2^n\|^2 + \|\Delta Q_3^n\|^2) + 2\epsilon^2\Delta t\|\Delta^2\bar{e}^{n+1}\|^2 + 2\epsilon^2\Delta t\|\Delta^2\bar{e}^n\|^2 \\
\le& C\Delta t\left(\|B_k(\bar{e}^n)\|^2 + \|\nabla B_k(\bar{e}^n)\|^2 + \|\Delta B_k(\bar{e}^n)\|^2 + \|\nabla\Delta B_k(\bar{e}^n)\|^2 + \|\Delta^2 B_k(\bar{e}^n)\|^2\right) \\
&+ C\Delta t^{2k}\int_{t^{n+1-k}}^{t^{n+1}}\|\frac{\partial^k u}{\partial t^k}(s)\|_{H^4}^2 ds + 2\epsilon^2\Delta t\|\Delta^2\bar{e}^{n+1}\|^2 + 2\epsilon^2\Delta t\|\Delta^2\bar{e}^n\|^2.
\end{aligned} \tag{A.8}$$

Data availability

Data will be made available on request.

References

[1] Schimperna Giulio, Wu Hao. On a class of sixth-order Cahn–Hilliard-type equations with logarithmic potential. SIAM J Math Anal 2020;52(5):5155–95.
[2] Zhang Chenhui, Ouyang Jie, Wang Cheng, Wise Steven M. Numerical comparison of modified-energy stable SAV-type schemes and classical BDF methods on benchmark problems for the functionalized Cahn-Hilliard equation. J Comput Phys 2020;423:109772.
[3] Kuwert Ernst, Schätzle Reiner. Gradient flow for the Willmore functional. Comm Anal Geom 2002;10(2):307–39.
[4] Bretin Elie, Masnou Simon, Oudet Edouard. Phase-field approximations of the Willmore functional and flow. Numer Math 2015;131:115–71.
[5] Du Qiang, Liu Chun, Ryham Rolf, Wang Xiaoqiang. A phase field formulation of the Willmore problem. Nonlinearity 2005;18(3):1249.
[6] Du Qiang, Liu Chun, Wang Xiaoqiang. A phase field approach in the numerical study of the elastic bending energy for vesicle membranes. J Comput Phys 2004;198(2):450–68.
[7] Chen Chuanjun, Yang Xiaofeng. Fast, provably unconditionally energy stable, and second-order accurate algorithms for the anisotropic Cahn–Hilliard model. Comput Methods Appl Mech Engrg 2019;351:35–59.
[8] Chen Ying, Lowengrub John, Shen Jie, Wang Cheng, Wise Steven. Efficient energy stable schemes for isotropic and strongly anisotropic Cahn–Hilliard systems with the Willmore regularization. J Comput Phys 2018;365:56–73.
[9] Yang Xiaofeng. Efficient schemes with unconditionally energy stability for the anisotropic Cahn-Hilliard equation using the stabilized-scalar augmented variable (S-SAV) approach. 2018, arXiv preprint arXiv:1804.02619.
[10] Gompper Gerhard, Schick Michael. Correlation between structural and interfacial properties of amphiphilic systems. Phys Rev Lett 1990;65(9):1116.

[11] Chen Wenbin, Jing Jianyu, Wu Hao. A uniquely solvable, positivity-preserving and unconditionally energy stable numerical scheme for the functionalized Cahn–Hilliard equation with logarithmic potential. J Sci Comput 2023;96(3):75.
[12] Cahn John W, Hilliard John E. Free energy of a nonuniform system. I. Interfacial free energy. J Chem Phys 1958;28(2):258–67.
[13] Chen Feng, Shen Jie. Efficient spectral-Galerkin methods for systems of coupled second-order equations and their applications. J Comput Phys 2012;231(15):5016–28.
[14] Jones Jaylan Stuart. Development of a fast and accurate time stepping scheme for the functionalized Cahn-Hilliard equation and application to a graphics processing unit. Michigan State University; 2013.
[15] Feng Wenqiang, Guan Zhen, Lowengrub John, Wang Cheng, Wise Steven M, Chen Ying. A uniquely solvable, energy stable numerical scheme for the functionalized Cahn–Hilliard equation and its convergence analysis. J Sci Comput 2018;76(3):1938–67.
[16] Zhang Chenhui, Ouyang Jie. Unconditionally energy stable second-order numerical schemes for the Functionalized Cahn–Hilliard gradient flow equation based on the SAV approach. Comput Math Appl 2021;84:16–38.
[17] Shen Jie, Xu Jie, Yang Jiang. The scalar auxiliary variable (SAV) approach for gradient flows. J Comput Phys 2018;353:407–16.
[18] Shen Jie. Efficient and accurate structure preserving schemes for complex nonlinear systems. In: Handbook of numerical analysis, vol. 20, Elsevier; 2019, p. 647–69.
[19] Huang Fukeng, Shen Jie. Stability and error analysis of a class of high-order IMEX schemes for Navier–Stokes equations with periodic boundary conditions. SIAM J Numer Anal 2021;59(6):2926–54.
[20] Huang Fukeng, Shen Jie. A new class of implicit–explicit BDFk SAV schemes for general dissipative systems and their error analysis. Comput Methods Appl Mech Engrg 2022;392:114718.
[21] Huang Fukeng, Shen Jie, Yang Zhiguo. A highly efficient and accurate new scalar auxiliary variable approach for gradient flows. SIAM J Sci Comput 2020;42(4):A2514–36.
[22] Temam Roger. Infinite-dimensional dynamical systems in mechanics and physics, vol. 68, Springer Science & Business Media; 2012.
[23] Fiorenza Alberto, Formica Maria Rosaria, Roskovec Tomáš G, Soudskỳ Filip. Detailed proof of classical Gagliardo–Nirenberg interpolation inequality with historical remarks. Z Für Anal Und Ihre Anwendungen 2021;40(2):217–36.
[24] Shen Jie, Tang Tao, Wang Li-Lian. Spectral methods: algorithms, analysis and applications, vol. 41, Springer Science & Business Media; 2011.
[25] Quarteroni Alfio, Valli Alberto. Numerical approximation of partial differential equations, vol. 23, Springer Science & Business Media; 2008.
[26] Nevanlinna Olavi, Odeh F. Multiplier techniques for linear multistep methods. Numer Funct Anal Optim 1981;3(4):377–423.
[27] Akrivis Georgios, Chen Minghua, Yu Fan, Zhou Zhi. The energy technique for the six-step BDF method. SIAM J Numer Anal 2021;59(5):2449–72.
[28] Gavish Nir, Jones Jaylan, Xu Zhengfu, Christlieb Andrew, Promislow Keith. Variational models of network formation and ion transport: applications to perfluorosulfonate ionomer membranes. Polymers 2012;4(1):630–55.
[29] Gavish Nir, Hayrapetyan Gurgen, Promislow Keith, Yang Li. Curvature driven flow of bi-layer interfaces. Phys D: Nonlinear Phenom 2011;240(7):675–93.
[30] Jain Sumeet, Bates Frank S. Consequences of nonergodicity in aqueous binary PEO- PB micellar dispersions. Macromolecules 2004;37(4):1511–23.
[31] Jain Sumeet, Bates Frank S. On the origins of morphological complexity in block copolymer surfactants. Science 2003;300(5618):460–4.
[32] Christlieb Andrew, Jones Jaylan, Promislow Keith, Wetton Brian, Willoughby Mark. High accuracy solutions to energy gradient flows from material science models. J Comput Phys 2014;257:193–215.
[33] Bendejacq D, Joanicot M, Ponsinet V. Pearling instabilities in water-dispersed copolymer cylinders with charged brushes. Eur Phys J E 2005;17(1):83–92.
[34] Feng Wenqiang, Guo Zhenlin, Lowengrub John S, Wise Steven M. A mass-conservative adaptive FAS multigrid solver for cell-centered finite difference methods on block-structured, locally-cartesian grids. J Comput Phys 2018;352:463–97.
[35] Doelman Arjen, Hayrapetyan Gurgen, Promislow Keith, Wetton Brian. Meander and pearling of single-curvature bilayer interfaces in the functionalized Cahn–Hilliard equation. SIAM J Math Anal 2014;46(6):3640–77.